ORP5/8 AND MIB/MICOS LINK ER-MITOCHONDRIA AND INTRAMITOCHONDRIAL CONTACTS FOR NON-VESICULAR TRANSPORT OF PHOSPHATIDYLSERINE

Leila Rochin[1,2*], Vera F. Monteiro-Cardoso[1,2*], Amita Arora[3], Audrey Houcine[4], Eeva Jääskeläinen[5], Annukka M. Kivelä[3], Cécile Sauvanet[1,2], Romain Le Bars[1,6], Eyra Marien[5], Jonas Dehairs[5], Julie Neveu[1,2], Naima El Khallouki[1,2], Elena Santonico[7], Johannes V. Swinnen[5], David Tareste[8], Vesa M. Olkkonen[3,9], and Francesca Giordano[1,2#]

[1] Institute for Integrative Biology of the Cell (I2BC), CEA, CNRS, Univ. Paris-Sud, Université Paris-Saclay, Gif-sur-Yvette cedex 91198, France.

[2] Inserm U1280, Gif-sur-Yvette cedex 91198, France.

[3] Minerva Foundation Institute for Medical Research, Biomedicum 2U, FI-00290 Helsinki, Finland

[4] Institut Jacques Monod, CNRS, UMR7592, Université Paris Diderot, Sorbonne Paris Cité, F-75013 Paris, France

[5] Laboratory of Lipid Metabolism and Cancer, Department of Oncology, KU Leuven, Leuven B-3000, Belgium.

[6] Imagerie-Gif, Light Microscopy Facility, Institute for Integrative Biology of the Cell (I2BC), CEA, CNRS, Univ. Paris-Sud, Université Paris-Saclay, Gif-sur-Yvette cedex 91198, France

[7] University of Rome Tor Vergata, via della ricerca scientifica, dipartimento di Biologia, 00133, Italy

[8] Institute of Psychiatry and Neuroscience of Paris (IPNP), Inserm UMR-S 1266, Université de Paris, Paris, France

[9] Department of Anatomy, Faculty of Medicine, FI-00014 University of Helsinki, Finland

* These authors contributed equally to this work

Correspondence to: francesca.giordano@i2bc.paris-saclay.fr

SUMMARY

Mitochondria are dynamic organelles essential for cell survival whose structural and functional integrity rely on selective and regulated transport of lipids from/to the endoplasmic reticulum (ER) and across the mitochondrial intermembrane space. As they are not connected by vesicular transport, the exchange of lipids between ER and mitochondria occurs at sites of close organelle apposition called membrane contact sites. However, the mechanisms and proteins involved in these processes are only beginning to emerge. Here, we show that the main physiological localization of the lipid transfer proteins ORP5 and ORP8 is at mitochondria-associated ER membranes (MAMs) subdomains, physically linked to the MIB/MICOS complexes that bridge the two mitochondrial membranes. We also show that ORP5/8 mediate non-vesicular transport of phosphatidylserine (PS) lipids from the ER to mitochondria by cooperating with the MIB/MICOS complexes. Overall our study reveals a novel physical and functional link between ER-mitochondria contacts involved in lipid transfer and intra-mitochondrial membranes contacts maintained by the MIB/MICOS complexes.

KEYWORDS

Membrane contact sites, MAM, ER, mitochondria, ORP, phosphatidylserine.

INTRODUCTION

Vesicular trafficking is the major pathway for transport of proteins and lipids between membranes. However, an alternative route, which is vesicle-independent, occurs at regions of close inter-organelle membrane proximity (within less than 30 nm) also called membrane contact sites (Scorrano, De Matteis et al., 2019). This route is particularly important to preserve membrane composition, integrity and identity of intracellular organelles such as mitochondria that are largely excluded from the classical vesicle-mediated trafficking pathway. Like other organelles, mitochondria can be closely associated with the endoplasmic reticulum (ER), the major site of lipid synthesis and the major intracellular calcium (Ca^{2+}) store. ER membrane subdomains closely apposed to mitochondria are called mitochondria-associated ER membranes (MAMs) and they facilitate the exchange of Ca^{2+} and lipids between the two organelles (Herrera-Cruz & Simmen, 2017, Tatsuta, Scharwey et al., 2014, Vance, 2014).

Mitochondria are involved in a plethora of cellular processes including energy production, lipid metabolism, Ca^{2+} homeostasis and apoptosis. To fulfill their numerous functions, mitochondria need to maintain a defined membrane composition by receiving essential lipids and lipid precursors from the ER through membrane contact sites (Giordano, 2018, Vance & Tasseva, 2013).

Increasing lines of evidence suggest that lipid transfer proteins (LTPs) play a major role in regulating the lipid composition of membranous organelles by facilitating non-vesicular lipid transport at membrane contact sites. In recent years, several tethering complexes with lipid transfer activity have been identified at membrane contact sites between the ER and other intracellular organelles as well as the plasma membrane (PM) in yeast and mammalian cells. However, our knowledge of how lipids are exchanged at ER-mitochondria membrane contact sites remains rudimentary, and the LTPs that localize

and function at these sites are just starting to be discovered. The best-studied lipid transfer/tethering complex at ER-mitochondria contact sites is the yeast ER-mitochondria encounter structure (ERMES) (Kornmann et al 2009, Lang et al 2015) that bridges the ER and the mitochondrial membranes and also facilitates the exchange of phospholipids (in particular phosphatidylcholine, PC) between them. In metazoans, very little is known on how lipids are exchanged at ER-mitochondria membrane contact sites and about the proteins involved in this process. Some tethers at mammalian ER-mitochondria contact sites have emerged in the recent years (Gatta and Levine 2017). However, none of these proteins has been directly involved in non-vesicular lipid transport between ER and mitochondrial membranes. Recently, mammalian LTPs with tethering function, such as VPS13A or Pdzd8 (the latter being proposed as a paralog of the ERMES subunit Mmm1(Wideman, Balacco et al., 2018)), were shown to localize at membrane contact sites, including those between ER and mitochondria, where they regulate membrane tethering and, in the case of Pdzd8, mitochondrial Ca^{2+} uptake (Hirabayashi, Kwon et al., 2017, Kumar, Leonzino et al., 2018). However, their function in lipid transport at these ER-mitochondria contacts has not been proven.

The Oxysterol binding protein (OSBP)-related proteins constitute a large family of LTPs conserved from yeast (Osh) to humans (ORP) and localized to different subcellular sites, shown in several cases to be membrane contact sites. A common feature of all ORPs is the presence of an OSBP-related lipid-binding/transfer (ORD) domain. Most ORP proteins contain a two phenylalanines (FF) in an acidic tract (FFAT)-motif that binds ER-localized VAP proteins and a pleckstrin homology (PH) domain that interacts with lipids or proteins in distinct non-ER organelle membranes. Two members of this family, ORP5 and ORP8, do not contain an FFAT motif but are directly anchored to the ER through a C-terminal transmembrane (TM) segment.

ORP5 and ORP8 have been previously shown to localize at ER-PM contact sites where they transfer phosphatidylserine (PS) from the cortical ER to the PM, in counter-exchange with the phosphoinositides Phosphatidylinositol-4-phosphate (PI4P) and Phosphatidylinositol 4,5-bisphosphate (PIP_2) (Chung et al. 2015; Ghai et al, 2017). We have recently shown that ORP5 and ORP8 are also present in the MAM and play a key role in maintaining mitochondrial integrity (Galmes, Houcine et al., 2016). We and others, have also shown that ORP5/8 form a protein complex in the cell (Chung, Torta et al., 2015, Galmes et al., 2016). However, ORP5 and ORP8, when overexpressed, display a different distribution within MCS. In particular, overexpression of ORP5 greatly expands ER-PM contacts (Chung et al., 2015, Galmes et al., 2016), resulting in an accumulation of ORP5 at these sites, while overexpressed ORP8 is largely retained in the reticular ER. As all the studies on ORP5 and ORP8 so far have employed their individual overexpression, the endogenous sites where ORP5 and ORP8 interact and function as a complex are still unknown.

Interestingly, transport of PS is a key event occurring at ER-mitochondria contact sites. Newly synthesized PS, by the ER-localized PS-Synthase 1 (PSS1), is shuttled from the ER to the outer mitochondrial membrane (OMM) and from OMM to inner mitochondrial membrane (IMM) where it is rapidly converted to phosphatidylethanolamine (PE) by the PS-decarboxylase enzyme PISD (Vance, 1990, Vance & Tasseva, 2013). At the IMM, PE plays crucial roles in maintaining mitochondrial tubular morphology and therefore mitochondrial respiratory functions (Joshi, Thompson et al., 2012, Steenbergen, Nanowski et al., 2005). Regardless of extensive studies on PS transport between ER and mitochondria since its first discovery more than 20 years ago (Vance, 1990), the underlying mechanisms and proteins involved are still elusive.

Membrane contact sites exist also between the OMM and the IMM and are mediated by the Mitochondrial Intermembrane space Bridging (MIB) and Mitochondrial Contact sites and Cristae junction Organizing System (MICOS) complexes. The MICOS complex is a multi-subunit complex preferentially located at Cristae Junctions (CJ), tubular structures that connect the IMM to the cristae, and it is necessary for CJ formation, cristae morphology and mitochondria function (Harner, Korner et al., 2011, Huynen, Muhlmeister et al., 2016, Ott, Dorsch et al., 2015, Wollweber, von der Malsburg et al., 2017). The integral IMM protein Mitofilin is the central component of the MICOS complex and carries a large domain exposed to the mitochondria intermembrane space (IMS) that interacts with the OMM Sorting and Assembly Machinery (SAM) to form the MIB complex (Friedman, Mourier et al., 2015, Guarani, McNeill et al., 2015). The SAM complex is constituted of SAM50 (a pore-forming β-barrel protein), Metaxin1 and 2, and is involved in the membrane insertion and assembly of mitochondrial β-barrel proteins (Hohr, Lindau et al., 2018, Kozjak, Wiedemann et al., 2003, Kozjak-Pavlovic, Ross et al., 2007). However, whether and how OMM-IMM contact sites are linked to ER-mitochondria contacts in mammalian cells is still largely unknown.

Here we uncover for the first time the endogenous localization of ORP5 and ORP8, revealing that the major site of their interaction in physiological conditions are the MAMs. We also show that the ER subdomains where ORP5 and ORP8 reside are physically connected to the intra-mitochondrial membrane contacts bridged by the MIB/MICOS complexes at cristae junctions. We then show that ORP5/8 cooperate with SAM50 and Mitofilin, key components of the MIB/MICOS complex, to mediate PS transport from the ER to the mitochondrial membranes at ER-mitochondria contact sites in mammalian cells, and consequently the synthesis of mitochondrial PE.

Our findings reveal a novel tripartite association between the ER and the two mitochondrial membranes that links lipid transfer across these membranes, cristae biogenesis and consequently mitochondria function.

RESULTS

ER-mitochondria contact sites are the main physiological localization of the ORP5-ORP8 complex

The localization of ORP5 and ORP8 at membrane contact sites at endogenous level is still unknown. We thus investigated the localization of endogenous ORP5 and ORP8 by immunofluorescence using antibodies against ORP5 and ORP8 proteins. First, we validated the specificity of these antibodies in cells overexpressing ORP5 or ORP8 proteins fused with a similar fluorescent tag (EGFP-ORP5 or EGFP-ORP8) and found that ORP5 and ORP8 signals detected using these antibodies co-localized with the overexpressed proteins (Fig. S1a-b). Then, we analyzed ORP5 and ORP8 endogenous localization in control HeLa cells and in cells where ORP5 and ORP8 were downregulated by RNAi and whose mitochondria were labeled by MitoTracker. We found a strong decrease in ORP5 and ORP8 labeling upon their knockdown, whose efficiency (of about 95-100%) was confirmed by WB (Fig. 1b), confirming the specificity of the used antibodies (Fig. 1a-c, S1a-b). Interestingly, in control conditions the majority of endogenous ORP5 and ORP8 co-localized to subcellular compartments in close proximity to mitochondria (Fig. 1a, 1d, 1e-f, S1c). ORP5 and ORP8-positive compartments overlapped with the ER protein RFP-Sec22b, confirming endogenous ORP5 and ORP8 localization to the ER and further validating the specificity of these antibodies (Fig. S1c).

We then sought to analyze ORP5 and ORP8 localization when co-overexpressed (at similar levels) by co-transfecting HA-ORP5 and EGFP-ORP8 in HeLa cells and comparing

their localization with the individually expressed ORP5 and ORP8 (EGFP-ORP5 or EGFP-ORP8) by confocal microscopy. When expressed alone, EGFP- ORP5 localizes to ER in contact with mitochondria, but also strongly increases ER-PM contact sites where it redistributes, while it localizes very little in the reticular ER (Fig. 1g, S1d and (Galmes et al., 2016)). Instead, EGFP-ORP8, when expressed alone, localizes mostly to ER-mitochondria contact sites and to reticular ER, with only a minor pool at cortical ER, as it does not increase ER-PM contact sites (Fig. 1g, S1d). Remarkably, even if the individually overexpressed ORP5 and ORP8 were differently distributed among MCS, their localization at ER-mitochondria contacts was higher as compared to a general ER protein, such as Sec22b (Fig. 1h). Moreover, and interestingly, when expressed together, ORP5 and ORP8 equally redistributed and co-localized to cortical ER, reticular ER and ER-mitochondria contacts (Fig. 1g, S1d). In particular, their localization to ER-mitochondria contacts was higher as compared to when expressed individually (Fig. 1h). Also, the co-localization of co-overexpressed ORP5 and ORP8 was comparable to the co-localization of the endogenous proteins, as revealed by the high Pearson's correlation coefficient that was in both cases close to 1 (Fig. 1f). These data indicate that co-expression of ORP5 and ORP8 mimics the physiological localization of these proteins as a complex, when the expression levels of one of the two proteins are not highly enriched as compared to the other.

To further analyze and quantify ORP5 and ORP8 co-localization and interaction at ER-mitochondria contact sites in co-overexpression and endogenous conditions we used Duolink-Proximity Ligation Assay (PLA) coupled with staining of mitochondria (MitoTracker) and confocal microscopy. PLA signals corresponding to ORP5-ORP8 interaction were observed throughout the cell in both endogenous and co-overexpression (HA-ORP5 and 3XFLAG-ORP8) conditions (Fig. 2a). The specificity of this assay and of

198 the antibodies used was confirmed by the strong decrease in PLA signals for endogenous
199 ORP5-ORP8 interaction in cells with ORP5 and ORP8 knocked down (Fig. 2b, S2a).
200 Likewise, a significant increase in ORP5-8 PLA signals was induced by the
201 overexpression of these proteins (Fig. 2b)

202 Close association of PLA spots to mitochondria, indicating localization at ER-
203 mitochondria contact sites, was measured after segmentation of the mitochondrial
204 network by Imaris (Fig. 2a, right panel; S2b). Interestingly, the majority of ORP5-8 PLA
205 signals localized at ER-mitochondria contact sites (52% of endogenous ORP5-8 and 50%
206 of co-overexpressed ORP5-8) (Fig. 2a, 2c). The localization of ORP5-8 PLA signals to
207 ER-PM contact sites was analyzed in HeLa cells transfected with RFP-PH-PLCδ, to stain
208 the PM, and Mito-BFP, to label mitochondria. However, only a minor pool of ORP5-8 PLA
209 spots was found in contact with the PM (4% of endogenous ORP5-8 and 5% of co-
210 overexpressed ORP5-8) (Fig. 2d-f). The localization of ORP5-ORP8 PLA spots to the ER,
211 including MAMs, was confirmed in cells co-expressing the ER protein Sec22b and the
212 mitochondrial-targeted Mito-BFP (Fig. S2c).

213 Overall these data reveal for the first time that the main sites where ORP5 and ORP8
214 localize and interact in physiological and endogenous conditions are the ER-mitochondria
215 contact sites, and not the ER-PM contacts.

216

217 **ORP5/8 physically interact with the mitochondrial intermembrane space**
218 **bridging (MIB) complex facing cristae junctions**

219 To investigate whether ORP5/8 localize to specific ER-mitochondria contact
220 subdomains we performed a morphological analysis of ORP5 localization by immuno-
221 EM (IEM) on ultrathin cryosections from HeLa cells transfected with HA-ORP5 or
222 EGFP-ORP5 (as endogenous ORP5/8 levels are too low to be detected by IEM). We

previously reported that about 20% of ORP5 or ORP8 gold particles were associated to ER-mitochondria contact sites when individually expressed (Galmes et al., 2016). The advantage of analyzing ORP5 localization is its preferential localization to contact sites, when expressed alone, as compared to ORP8 (Galmes et al., 2016), which remains also largely present within the reticular ER. Interestingly, the majority of ORP5 gold particles was found to localize to ER elements in a very close proximity (86% within 0-100 nm distances, 50% of which within 50 nm) to the CJ (arrow, Fig. 3a-b), tubular structures that connect the IMM to the cristae. To exclude that ORP5 localization near CJ is not a consequence of its distribution throughout the ER membranes, we sought to determine if other ER proteins have a similar frequency of proximity to CJ. Thus, we compared ORP5 localization to Sec61β, a subunit of the Sec61 complex involved in protein translocation in the ER, which is present in ER elements distributed throughout the cells and very little at ER-mitochondria contact sites (Galmes et al., 2016). Co-immunolabeling of EGFP-ORP5 or EGFP-Sec61β and protein disulfide isomerase (PDI) to stain the ER, confirmed ORP5 localization in ER elements close to CJ (arrow, Fig. 3c) but not of Sec61β, the bulk of which localized on ER membranes distant from the CJ (0% within 0-100nm and 69% >200nm distance) even when close to mitochondria (Fig. 3b and arrowheads in Fig. 3c). Hence, our results support the conclusion that ORP5 specifically localizes to ER-mitochondria contact sites closely associated to CJ. Interestingly, in yeast, CJ were shown to be closely associated to OMM-IMM contact sites tethered by the MICOS complex (Harner et al., 2011). IEM analysis using Mitofilin-EGFP, an EGFP-tagged construct of the human orthologue of the central component of the MICOS complex, confirmed that human Mitofilin, similarly to its yeast orthologue, preferentially localizes to the IMM in close proximity of CJ and in the cristae that arise from them (arrow, Fig. 3a). These

results suggest that ER-mitochondria contact sites where ORP5/8 localize could be physically connected to the intra-mitochondrial membrane contact sites near CJ.

To identify binding partners of ORP5/8 at ER-mitochondria contact sites we carried out a MS-analysis on GFP-pull downs from cells expressing EGFP-ORP5, EGFP-ORP5ΔPH (an ORP5 variant lacking the PM-targeting PH domain that is localized at ER-mitochondria but not at ER-PM contact sites)(Fig. S3b), or EGFP alone as a control (Fig. 4a). As expected, the highest hit detected in both EGFP-ORP5 and EGFP-ORP5ΔPH pull-downs was ORP8. In accord to our previous study (Galmes et al., 2016), the mitochondrial protein PTPIP51 was also detected in the mass spectrometry analysis. Interestingly, several new outer mitochondrial membrane proteins (listed in Fig. 4a) were also found as major hits. Among these proteins the Sorting Assembly Machinery Subunit 50 (SAM50), a central component of the SAM protein complex involved in the import and assembly of mitochondria β-barrel proteins in the OMM (Hohr et al., 2018), had one of the highest scores (Fig. 4a).

SAM50 is part of the Mitochondrial intermembrane space bridging (MIB) complex, composed of metaxin-1, metaxin-2 and the MICOS complex that anchors the OMM to the IMM at CJ (Huynen et al., 2016, Ott et al., 2015). SAM50 is also known to directly bind the central component of the MICOS complex Mitofilin (Ott et al., 2015). Consistently, Mitofilin was also detected in the MS of EGFP-ORP5 and EGFP-ORP5ΔPH pull-downs (Fig. 4a). Interestingly, SAM50 and Mitofilin showed a higher interaction score in EGFP-ORP5ΔPH immunoprecipitates, as compared to EGFP-ORP5. To verify that the overexpression of ORP5 or ORP5ΔPH did not affect the protein levels of SAM50 and Mitofilin, WB analysis using anti-actin as loading control was carried out on cells expressing EGFP-ORP5, EGFP-ORP5ΔPH or EGFP alone. Our results show that neither EGFP-ORP5 nor EGFP-ORP5ΔPH overexpression

alters the amount of SAM50 and Mitofilin proteins as compared to the overexpression of EGFP alone (Fig. 4b). Of note, metaxin-2, and RHOT2, other components of the MIB/MICOS complex, localized to the outer mitochondrial membrane, were also detected in the MS of immunoprecipitated EGFP-ORP5 and EGFP-ORP5ΔPH, although the score of metaxin-2 in the EGFP-ORP5 was lower than the assigned threshold (50) (Fig. 4a).

To confirm ORP5/8 interaction with SAM50 and Mitofilin, GFP-pull down experiments from HeLa cells expressing EGFP-ORP5, EGFP-ORP8 or EGFP alone were carried out (Fig. 4c). Consistent with the MS data, endogenous SAM50 and Mitofilin were recovered with both EGFP-ORP5 and EGFP-ORP8 but not with EGFP alone, confirming specific interaction of ORP5 and ORP8 with SAM50 and Mitofilin.

Next, to determine the domains involved in the interaction of ORP5/8 with the MIB/MICOS complex, GFP-pull down experiments were carried out from cells expressing EGFP-tagged ORP5 (EGFP-ORP5ΔPH) or ORP8 (EGFP-ORP8ΔPH) PH domain deleted constructs (Fig. S3b), and compared to the full-length proteins (EGFP-ORP5 and EGFP-ORP8) or to the EGFP alone. In accord with the MS data, the deletion of the PH domain increased ORP5 and ORP8 interaction with SAM50, as compared to the full-length proteins (Fig. 4d). Confocal analysis of ORP5 and SAM50 localization on cells expressing EGFP-ORP5 or EGFP-ORP5ΔPH and stained with an anti-SAM50 antibody confirmed the stronger enrichment of the ΔPH ORP5 construct at ER elements in contact with the SAM50-labeled mitochondria as compared to the full-length ORP5 (Fig. S3a).

As the PH domain is not required for the interaction with SAM50, we further investigated the role of the other domains of ORP5 in such interaction by immunoprecipitating ORP5 deletion mutants for the ORD or the TM domains (EGFP-

298 ORP5ΔORD, EGFP-ORP5ΔTM) (Fig. S3b, Fig. 4d). While the deletion of the ORD
299 domain did not affect the interaction between ORP5 and SAM50, the deletion of the
300 TM domain decreased the amount of SAM50 co-immunoprecipitated with ORP5,
301 indicating that ORP5 should be properly anchored to the ER to localize at ER-
302 mitochondria contact sites and to interact with SAM50 (Fig. 4d).

303 To confirm the interaction between ORP5/8 and SAM50 at endogenous level, as
304 an anti-ORP5 antibody from a different specie than SAM50 was not available, we took
305 advantage of the available antibodies against ORP8 and SAM50 from different species
306 and analyzed their interaction using PLA (duolink) by confocal imaging in control HeLa
307 cells and in cells where SAM50 was downregulated by RNAi (siSAM50). PLA signals
308 corresponding to ORP8-SAM50 endogenous interaction were detected at ER-
309 mitochondria contact sites in control cells (Fig. 4e). Also, a decrease of about 40% of
310 ORP8-SAM50 PLA was found in siSAM50 cells, in accord with the decrease of the
311 levels of SAM50 protein of about 40-50% assessed by WB, and validating the
312 specificity of ORP8-SAM50 interaction (Fig. 4e-g).

313 To investigate a possible role of SAM50 and Mitofilin in regulating the levels of
314 ORP5/8 at MAMs we analyzed their endogenous interaction by PLA and confocal
315 microscopy in HeLa cells where either SAM50 or Mitofilin were knocked-down by
316 siRNA oligos. Interestingly, a significant decrease (of about 40%) in ORP5/8 interaction
317 was found in both SAM50- and Mitofilin-knockdown cells, as compared to control cells
318 (Fig. 5a-b), indicating a synergistic effect of SAM50/mitofilin on ORP5-ORP8
319 interaction.

320 To verify the possibility of an indirect effect of SAM50 or Mitofilin silencing on the
321 morphology and abundance of MAMs we carried out an ultrastructural analysis by
322 conventional EM and HRP-KDEL EM (carrying a horseradish peroxidase (HRP) tagged

with an ER retention motif to stain the ER) in Mitofilin or SAM50 silenced cells. Morphological analysis by conventional EM showed that transient (48 hours) knockdowns of SAM50 or Mitofilin induce formation of multilamellar cristae, almost devoid of CJ (Fig. S4a-b), complementing previous observations by other groups through stable disruption of the MICOS/MIB functions (Ding, Wu et al., 2015, Ott et al., 2015). However, in both SAM50 and Mitofilin knockdown cells ER-mitochondria contact sites were still present and their morphology not altered (Fig. 5c-d). Quantitative morphological analysis by HRP-KDEL EM in control and SAM50 or Mitofilin silenced cells confirmed that the abundance of ER-mitochondria contact sites was not altered by SAM50 or Mitofilin knockdown (Fig. 5c-d), indicating that the effects on ORP5/8 interaction at MAMs were not indirectly due to a global rearrangement of the ER-mitochondria contact sites.

Overall our data reveal a novel interaction between ORP5/8 and the MIB/MICOS complex at ER subdomains associated to intra-mitochondrial membrane contacts facing CJ, and a direct role of the MIB/MICOS complex in ORP5/8 targeting/interaction at MAMs.

ORP5/8 and the MIB/MICOS complex regulate PS-to-PE conversion at the ER-mitochondria interface

ORP5 and ORP8 role in lipid transport at ER-mitochondria contacts still remains to be established. We hypothesized that ORP5 and ORP8 could mediate PS transport at the ER-mitochondria interface. As the ER-derived PS is the major precursor for mitochondrial PE, if ORP5 and ORP8 mediate non-vesicular transport of PS from the ER to the mitochondria, then their absence should lead to a reduction of mitochondrial PE.

To test whether ORP5 and ORP8 regulate levels of mitochondrial PE *in situ*, we used Percoll gradient-based subcellular fractionation (as in (Galmes et al., 2016)) to isolate pure mitochondria from HeLa cells where ORP5 or ORP8 were transiently silenced by RNAi. We chose to use a transient knockdown as it overcomes the limits and/or compensatory effects on lipid transport/biosynthetic pathways that other stable approaches could induce. The purity of mitochondria and of the other subcellular fractions was verified in control, ORP5 and ORP8 knockdown conditions by western blotting (WB) (Fig. 6a). As controls for the purity of subcellular fractions, the samples were probed for cytochrome c as mitochondrial marker and IP3R-3 as a MAM-enriched marker. All markers were highly enriched in their respective fractions and were absent in the others. In accord with our previous study (Galmes et al., 2016), ORP5 and ORP8 were enriched in the MAM fraction and absent in the mitochondria fraction of control cells (Fig. 6a). On the contrary, they were strongly suppressed in ORP5 and ORP8 knockdown cell lysates and in the respective MAM fractions (Fig. 6a). The PE content of purified mitochondria from ORP5 and ORP8 knockdown was then analyzed by mass spectrometry (MS)-based lipidomics, which revealed a reduction of PE levels in mitochondria isolated from ORP5 and ORP8 knockdown cells of 34% and 20%, respectively, as compared to control cells (Fig. 6b). Interestingly, PE levels of the total cells were unchanged, indicating a specific effect of ORP5 or ORP8 depletion on mitochondrial PE. These data suggest that ORP5 and ORP8 could transfer PS at ER-mitochondria contact sites.

We, then, sought to investigate the ability of ORP5 and ORP8 ORD domains (ORD5 and ORD8) to transfer PS *in vitro*. So far, only the ORD of ORP8 has been studied for its lipid transfer activity *in vitro*, and it has been shown to transfer PS between liposome membranes in counter-transport with PI4P or PIP_2 *in vitro* (Chung et al. 2015;

Ghai et al, 2017). However, the *in vitro* lipid transfer activity of ORP5 ORD domain has not been studied yet. Also, no study so far has addressed either the ability of ORD5 and ORD8 to transfer PS in the absence of a gradient of PI4P or PIP_2 or other phospholipids than PS between liposomes *in vitro*. Thus, to compare and study their role in the transfer of phospholipids *in vitro*, we purified the recombinant ORD5 (aa 265-703) and ORD8 (aa 328-767) from bacteria (Escherichia coli) (Fig. S5a) and measured their ability to transport fluorescent phospholipids (TopFluor-PS, -PC or -PE) from donor to acceptor liposomes *in vitro*. Donor liposomes containing fluorescent phospholipids and biotinylated lipids (liposomes composed of 1 mol% TopFluor-PS, -PC or -PE, 2 mol% biotinylated-PE, and 97 mol% POPC) were first immobilized on streptavidin beads and then mixed with acceptor liposomes (composed of 100 mol% POPC) in the presence or absence of ORP5/8 ORD domains (Fig. S5b). After 1 hour at 37°C, acceptor liposomes were recovered from the supernatant and their fluorescence was measured (Fig. S5b). Our results show that both ORD5 and ORD8 transfer PS, but not PC and PE, from donor to acceptor liposomes (Fig. S5c). They also reveal that ORD5 and ORD8 share equivalent ability to transfer PS *in vitro*. To confirm that fluorescent lipids were indeed transferred to the acceptor liposomes, a fraction of the reaction supernatant was floated on a Nycodenz density gradient by ultracentrifugation and the fluorescence in the top fraction of the gradient (containing floated acceptor liposomes) was measured (Fig. S5d). Fluorescence of TopFluor-PS in the acceptor liposomes was maintained after their floatation, confirming its effective transfer between liposomes *in vitro*.

In subsequent experiments, we measured the levels of mitochondrial PE newly synthesized from the ER-derived PS by using a radiometric PS-to-PE conversion assay *in situ* (Shiao, Lupo et al., 1995) in silenced or control HeLa cells (Fig. 6c). This assay allows the monitoring of PS transfer from the ER to mitochondria by measuring

the levels of radioactive PS and PS-derived PE by thin layer chromatography (TLC) after 18h of incorporation of radioactive L-[^{3}H(G)]-serine into the cells. A significant decrease in the levels of newly synthetized PE was found in ORP5 knockdown and in ORP5+ORP8 double-knockdown cells (Fig. 6c). The decrease was stronger in ORP5+ORP8 double-knockdown cells, indicating a cooperative effect of ORP5 and ORP8 in this process. A slight, not statistically significant decrease was also found in ORP8 knockdown cells, suggesting a major role of ORP5 compared to ORP8 in PS transfer at ER-mitochondria contact sites *in situ*. As [^{3}H]-serine radioactivity could be incorporated to PE also *via* an alternative pathway involving sphingosine (Hanada, Nishijima et al., 1992), we next sought to address the contribution of this pathway to PE labeling, by repeating the experiments in control and ORP5 knockdown cells in the presence of β-chloro-L-alanine, an inhibitor of serine palmitoyltransferase (Chen, Born et al., 1993). The PS-to-PE conversion was not significantly affected in both control (~3% of reduction) and ORP5 knockdown cells (~9% of reduction). On the contrary, PS-to-PE conversion was significantly reduced in β-chloro-L-alanine treated and untreated ORP5 knockdown cells (~17% and ~23% respectively), as compared to control (Fig. 6d). These data show that more than 90% of the serine labeling of PE occurs via PS in HeLa cells, in accord with a previous work in another cell type, the Baby Hamster Kidney fibroblasts (BHK cells), showing that only a minor PE species are labeled from the sphingosine-PE pathway (Heikinheimo & Somerharju, 1998). Additionally, the decrease in PE could be due to a decrease in the protein levels of the PS-decarboxylase (PISD) or the PS-Synthase 1 (PSS1) enzymes mediating PS-to-PE conversion on mitochondria or PS synthesis in the ER, respectively. To exclude this possibility we analyzed the protein levels of PISD and PSS1 by WB in ORP5, ORP8, ORP5+ORP8 knockdown cells and compared them to control cells (Fig. S5e). We

found no significant difference but rather a slight increase in the enzymes upon ORP5 and/or ORP8 knockdowns. Overall these data confirm that the reduction in mitochondrial PE induced by depletion of ORP5 is essentially due to the decrease in PS transfer from the ER to the mitochondria (Fig. S5g).

Even a modest reduction (22-27%) of mitochondrial PE levels in mammalian cells has been shown to profoundly alter the morphology of mitochondrial cristae as well as mitochondria functions (Tasseva, Bai et al., 2013). Accordingly, ORP5 and ORP8 knockdowns lead to alterations of mitochondria morphology (Galmes et al., 2016). However, the impact of ORP5 and ORP8 knockdowns on the abundance of ER-mitochondria contact sites remain unclear.

To test whether the effects on PS transport at ER-mitochondria contacts were specific for ORP5 and ORP8 loss of function or simply due to a decrease of ER-mitochondria contacts induced by their knockdown, we quantified the abundance of ER-mitochondria contact sites by EM in control and ORP5, ORP8, ORP5+ORP8 knockdown cells. To facilitate the visualization of the ER we transfected the cells with a HRP-KDEL construct that stains the ER with a dark signal. Our quantifications revealed that ORP5, ORP8 or ORP5+ORP8 knockdowns did not affect the extent of ER-mitochondria contact sites (Fig. 6e-f). These results indicate that ORP5 and ORP8 act as LTPs rather than tethers (Fig. 7, S5g). Additionally, 52% of mitochondria in ORP5+ORP8 double-knockdown cells display aberrant cristae morphology versus 9% in control cells (Fig. 6e, S5f). These defects in cristae morphology were also observed by conventional EM (Fig. S4a) and were similar to those previously shown in the case of ORP5 and ORP8 individual knockdowns (Galmes et al., 2016). However, the % of mitochondria with altered morphology in ORP5+ORP8 double-knockdown cells was higher as compared to ORP8 knockdown (Galmes et al., 2016), possibly reflecting the

stronger effect of ORP5+ORP8 double-knockdown on PS transport at ER-mitochondria contact sites (Fig. 6c).

Decreased levels of PE strongly affect the organization of the mitochondrial respiratory supercomplexes (Tasseva et al., 2013). We had previously shown that ORP5 knockdown induces a reduction in the basal mitochondrial oxygen consumption rate (OCR_{BAS}), indicative of reduced respiratory activity (Galmes et al., 2016). However, it remains still questioned whether ORP8 could also reduce OCR_{BAS} and/or if this reduction could be exacerbated under metabolic stress conditions. Thus, we monitored mitochondrial OCR in control, in ORP5 and in ORP8 knockdown cells in basal and in stress conditions (Fig. S6). ORP5 knockdown induced a significant reduction in both OCR_{BAS} (~37%) and OCR upon FCCP treatment (OCR_{FCCP}) (~36%). Interestingly, also ORP8 knockdown induced a significant decrease in OCR_{BAS} (~31%) and OCR_{FCCP} (~29%), although the decreases were less prominent than upon ORP5 knockdown. These data uncover a novel role of ORP5 and ORP8 in preserving mitochondrial respiratory activity in basal and in stress conditions, and a major impact of ORP5 in this process, in accord with its major role in PS transfer at ER-mitochondria contact sites.

To test whether the interaction of ORP5 with the MIB complex could facilitate the non-vesicular transfer of PS from the ER to the mitochondrial membranes (and consequently synthesis of mitochondrial PE) we depleted ORP5, SAM50 or Mitofilin alone or in combination by RNAi and analyzed the content in mitochondrial PE newly synthesized from PS using the same radiometric PS-to-PE conversion assay *in situ* as described above. Robust knockdown of ORP5, SAM50 or Mitofilin was confirmed by western blotting after 48 hours (Fig. 6g). Analysis of PS-derived newly synthetized PE revealed a significant decrease in PE in ORP5 and Mitofilin

knockdown cells (Fig. 6h). Moreover, the double-knockdown of ORP5 and Mitofilin had an additive effect, supporting a cooperation of these two proteins in the same process (PS transport/PE synthesis). However, the levels of PE were not changed in SAM50 knockdown cells as compared to control. This can be explained by the fact that other subunits of the MIB complex (*i.e.* Mitofilin) might compensate for its depletion. Indeed, protein levels of Mitofilin are increased in SAM50 knockdown cells (Fig. 6g). Interestingly, also the levels of both ORP5 protein and RNA are increased in SAM50 knockdown cells (Fig. 6g, S3b). Accordingly, the double-silencing of SAM50 and either ORP5 or Mitofilin had a significant impact on PE synthesis (Fig. 6h). Moreover, the reduction in PE was even stronger as compared to the individual knockdowns indicating that disruption of both a component implicated in a direct transport of PS at ER-mitochondria contact sites and a component of the OMM-IMM tethering complex has a significant impact on PE synthesis.

Morphological analysis by conventional EM in all these knockdown conditions was carried out, showing that transient double-knockdowns of ORP5+Mitofilin, ORP5+SAM50 and SAM50+Mitofilin, similarly to the individual knockdowns of SAM50 and Mitofilin, induces formation of multilamellar cristae, almost devoid of CJ (Fig. S4a-b). However, in all double-knockdown conditions analyzed ER-mitochondria contact sites were still present and their morphology not altered, as shown for the individual knockdowns of ORP5/8 (Fig. 6f), SAM50 and Mitofilin (Fig. 5c-d), indicating that the effects on PS-derived PE synthesis were specifically due to Mitofilin or SAM50 loss of function effects on intra-mitochondrial membrane bridges.

Overall our results reveal that ORP5/8 cooperate with the MIB/MICOS complex to regulate the transfer of PS from the ER to the mitochondrial membranes necessary for

498 synthesis of mitochondrial PE and consequently for maintaining mitochondrial cristae
499 morphology and respiration (Fig. 7).
500
501 **DISCUSSION**
502 In this study, by using a combination of biochemical and imaging approaches, we
503 uncover for the first time the endogenous localization of ORP5 and ORP8, revealing that
504 they are mainly localized at ER-mitochondria contact sites (Fig. 1-2 and Fig. S1-2), and
505 providing novel evidence for a physiological relevance of the ORP5/8 complex at MAMs.
506 So far, ORP5 and ORP8 localization have been only studied in conditions where one of
507 these two partner proteins were expressed in high excess as compared to the other one.
508 Previous studies, including one from our group, have shown that overexpression of ORP5
509 induces an increase of ER-PM contacts where the protein also localizes (Chung et al.,
510 2015, Galmes et al., 2016). Consequently, several following studies have addressed the
511 role of ORP5 and ORP8 at ER-PM contacts, overlooking their function at MAM. However,
512 the increase in cortical ER observed upon ORP5 overexpression does not reflect the
513 physiological abundance of ER-PM contacts, as the cortical ER in non-specialized cells
514 generally covers not more than 5% of the plasma membrane surface. Indeed, we have
515 found that the increased localization of ORP5 to cortical ER when over-expressed alone
516 does not reflect its endogenous localization when it is in complex with ORP8, which is
517 instead enriched at MAMs. Our findings have important implications for a better
518 understanding of the physiological localization and function of ORP proteins, but also of
519 other proteins that assemble in multimeric complexes at ER-mediated membrane contact
520 sites, such as the E-Syts (Giordano, Saheki et al., 2013).
521 Our study also reveals that ORP5/8 physically interact with SAM50 and Mitofilin,
522 two key components of the MIB/MICOS complex that anchor the IMM to the OMM at the

level of CJ (Huynen et al., 2016, Ott et al., 2015, Wollweber et al., 2017). The biochemical interaction between ORP5 and SAM50/Mitofilin uncovers the existence of a novel physical link between ER-mitochondria contact sites involved in lipid transport and intra-mitochondrial membrane contacts. ORP5 localization by IEM at ER-mitochondria contact sites near the CJ, where Mitofilin and MICOS complex also reside, further confirms the existence of such tripartite membrane contact site structure. Moreover, knockdown of SAM50 and Mitofilin does not affect ER-mitochondria contact sites, but perturbs the interaction of ORP5/8 at MAMs.

Importantly, here we describe a new function of ORP5 and ORP8 in the maintenance of mitochondrial levels of PE, an essential phospholipid of mitochondria, providing the first evidence of mammalian LTPs directly mediating non-vesicular transfer of PS (lipid precursor of mitochondrial PE) from the MAMs to the mitochondria at ER-mitochondria contact sites.

In yeast, large tethering complexes such as the ERMES and the ER-Membrane protein Complex (EMC) have been previously involved in phospholipid trafficking (PC and PS, respectively) between the ER and the mitochondrial membranes (Tamura & Endo, 2017) (Lang, John Peter et al., 2015). For instance, three subunits of the ERMES complex contain a Synaptotagmin-like Mitochondria lipid binding Protein (SMP) domain that forms a hydrophobic lipid transport cavity shared by other proteins of the tubular lipid-binding protein TULIP superfamily (Kopec, Alva et al., 2010, Reinisch & De Camilli, 2016). However, a direct role (independent of its tethering function) of ERMES in lipid transport at ER-mitochondria contact sites is still questioned. For a long time homologues of the ERMES complex have not been identified in metazoans. Hirabayashi et al. recently showed that the SMP-containing protein PDZD8 is involved in ER-mitochondria tethering and in the regulation of Ca^{2+}

548 dynamics in mammalian neurons (Hirabayashi et al., 2017). Although PDZD8 is a
549 structural and functional paralogous of the Mmm1 subunit of the ERMES complex
550 (Wideman et al., 2018), its function in lipid transport at ER-mitochondria contact sites
551 remain unclear. The EMC complex, which has been involved in PS shuttling at ER-
552 mitochondria contact sites in yeast, is instead highly conserved in metazoans
553 (Wideman, 2015). However, no lipid-binding/transfer domain has been found in the
554 EMC proteins, indicating that their implication in lipid transfer at ER-mitochondria
555 contacts is linked to their tethering function rather than to a direct lipid transfer activity.
556 Recently, the mammalian LTP VPS13A has been shown to localize to contact sites
557 including ER-mitochondria contacts (Kumar et al., 2018). VPS13A contains a lipid-
558 binding domain (VPS13α) that has the ability to harbor multiple phospholipids at once
559 and transfer them between liposomes *in vitro*. However, its role in lipid transfer at ER-
560 mitochondria membrane contact sites *in situ* has not yet been established. Differently
561 from the SMP and VPS13α domains that can simultaneously host multiple
562 phospholipids, the ORD domain of Osh/ORPs forms a cavity that can host only one
563 lipid at a time (Maeda, Anand et al., 2013, Wang, Ma et al., 2019).

564 An important finding of our work is that ORP5 and ORP8 knockdowns do not affect
565 the extent of ER-mitochondria contact sites, revealing that the main function of ORP5/8
566 at MAMs is lipid transfer and not membrane tethering. This is a unique feature among
567 the LTPs that have been identified so far at MAMs. For instance, knockdowns of other
568 LTPs such as ERMES in yeast, or PDZD8 and VPS13A in mammals, result in a
569 decrease of ER-mitochondria contact sites (Hirabayashi et al., 2017, Kornmann, Currie
570 et al., 2009, Kumar et al., 2018), making difficult to dissect the lipid transfer activity
571 from the tethering function of these LTPs. Thus, ORP5/8 represent so far a unique
572 example of LTPs that specifically mediate lipid transport at ER-mitochondria contact

573 sites, independently of membrane tethering, and that can be used as unique tools to
574 specifically study lipid transport at MAMs.

575 ORP5 and ORP8 have been previously shown to counter-exchange PS with the PM
576 phosphoinositides PI4P and PIP_2 at ER-PM contact sites in HeLa cells (Chung et al.,
577 2015, Ghai, Du et al., 2017). However, PI4P and PIP_2 are not present on the
578 mitochondrial membranes, while PE is highly abundant in these membranes, in
579 addition to being an essential lipid of all biological membranes. Our *in vitro* data show
580 that the ORD domains of ORP5 and ORP8 transport PS, but not other phospholipids such
581 as PE and PC, indicating a specific role of ORP5/8 in PS transport and excluding the
582 possibility that ORP5/8 might also participate in the transport of a fraction of PE back
583 to the ER. It is possible that ORP5/8 cooperate with other LTPs, such as VPS13A, for the
584 exchange of other lipids (including PE) at ER-mitochondria contact sites. Importantly,
585 we have confirmed the role of ORP5/8 in PS transfer by measuring a decrease of PS-
586 derived mitochondrial PE in ORP5 depleted HeLa cells *in situ* (and even more upon
587 ORP5+8 silencing) as well as a reduction of total PE in mitochondria isolated from
588 these cells (Fig. 6a-d). Accordingly, the knockdown of ORP5/8 affects cristae
589 morphology and the respiratory function of mitochondria (Galmes et al., 2016)(Fig. 6e-
590 f, S6), all phenotypes that are expected in the case of decrease in mitochondrial PE
591 (Joshi et al., 2012, Steenbergen et al., 2005). Our data further confirm the essential
592 role of PE in the maintenance of mitochondrial structure and functions, and are in
593 accord with those of (Tasseva et al., 2013) showing that even a mild decrease of
594 mitochondrial PE can strongly alter mitochondrial cristae morphology and respiratory
595 function. Our data also suggest that the gradient of PS at ER-mitochondria contacts is
596 sufficient to trigger the ORP5/8-mediated transport of PS from the MAMs, where it is
597 highly enriched, to the mitochondria membranes, where it is rapidly converted into PE

598 and is therefore present at a very low concentration. Our findings have important
599 implications in the general field of LTPs, as they suggest that the same LTP can use
600 different means to transfer lipids depending on the local gradients present at the
601 specific membrane contact sites where it is localized.

602 Importantly, we also show that the *de-novo* synthesis of mitochondrial PE requires
603 both ORP5/8 at ER-mitochondria contact sites and the MIB/MICOS complex at intra-
604 mitochondrial OMM-IMM contact sites (Fig. 6h). Interestingly, recent evidence in yeast
605 suggests that, in addition to the classical PE synthesis at the IMM by the IMM-localized
606 PS-decarboxylase PISD, PE can also be synthesized *in trans* on the OMM (Aaltonen,
607 Friedman et al., 2016). Thus, it is possible that this alternative pathway, which requires
608 MIB/MICOS tethering function to bring the mitochondrial intermembrane domain of
609 PISD close to the OMM for synthesis of PE, is conserved also in mammalian cells. The
610 cooperation of ORP5 with SAM50 and Mitofilin could facilitate the movement of PS from
611 the ER to the IMM across ER-mitochondria contact sites for synthesis of PE at the
612 IMM, through the classical PE synthesis pathway, but also PISD function *in trans* on
613 the OMM through this alternative biosynthetic pathway. Taken together these findings
614 provide the first evidence of a physical and functional link between ER-mitochondria
615 contacts and intra-mitochondrial membranes contacts maintained by the MIB/MICOS
616 complexes, to facilitate transport of PS from the ER to the mitochondria and PE
617 synthesis on the mitochondrial membranes (Fig. 7).

618 In conclusion, our data reveal that: 1) ORP5/8 form a protein complex that is
619 endogenously enriched at ER-mitochondria contacts; 2) ORP5/8 constitute the molecular
620 machinery mediating PS transfer at ER-mitochondria contact sites but not ER-
621 mitochondria tethering; 3) ER-mitochondria contacts where ORP5/8 localize are
622 physically associated with intra-mitochondrial contacts, maintained by the MIB/MICOS

623 complex, to facilitate the transport of PS from the ER to mitochondria membranes.
624 Overall our study provides a first molecular clue on how lipids are transported at ER-
625 mitochondria contact sites and novel functional insight into the complex interplay of the
626 ER with the mitochondria and the intra-mitochondrial membrane contacts and associated
627 machinery.
628
629 **METHODS**

630 **Cell culture, siRNA and transfection**.
631 HeLa cells were cultured in DMEM (Life Technologies) containing GlutaMax (Life
632 Technologies) and supplemented with 10% FBS (Life Technologies) and 1%
633 penicillin/streptomycin (Life Technologies) at 37°C and 5% CO_2. Transfection of
634 plasmids and siRNA oligos (Dharmacon, GE Healthcare) was carried out with
635 lipofectamine 2000 and oligofectamine (Life Technologies) according to
636 manufacturer's instructions.
637
638 **siRNAs oligonucleotides**
639 For knockdowns, HeLa cells were transfected with siRNA oligos by using
640 oligofectamine (Life Technologies) and cultured for 48 hours prior to analysis.
641 Double-stranded siRNAs were derived from the following references:

siRNA	Company, Reference
OSBPL8	Dharmacon, J-009508-06 (Galmes et al., 2016)
OSBPL8	Dharmacon, J-009508-05 (Galmes et al., 2016)
OSBPL5	Dharmacon, J-009274-10 (Galmes et al., 2016)
OSBPL5	Dharmacon, J-009274-11 (Galmes et al., 2016)

SAMM50	Dharmacon, J-017871-18
SAMM50	Dharmacon, J-017871-19
Non-targeting	Dharmacon, D-001810-10
siMitofilin	5’ - AAUUGCUGGAGCUGGCCUUTT-3’ (John, Shang et al., 2005)

642

643 **Plasmids and cDNA clones**

644 EGFP-ORP5, EGFP-ORP8, EGFP-ORP5ΔPH, EGFP-ORP8ΔPH, EGFP-
645 ORP5ΔORD and EGFP-ORP5ΔTM were described in (Galmes et al., 2016). GFP-
646 Sec22b and RFP-Sec22b (Gallo, Danglot et al., 2020). The following reagents were
647 kind gifts: GFP-Sec61β from T. Rapoport (Harward University)(Shibata, Voss et al.,
648 2008), PHPLCδ-RFP (Chung et al., 2015); Mito-BFP (Addgene: # 49151); ssHRP-
649 KDEL from T. Schikorski (Schikorski, Young et al., 2007); GST-ORD8 (ORD ORP8,
650 corresponding to aa 328-767) from P. De Camilli (Chung et al., 2015). GECO
651 constructs were from Robert Campbell (Addgene: CMV-R-GECO1 # 32444, CMV-
652 mito-R-GECO1 # 46021, CMV-ER-LAR-GECO1 # 61244, CMV-mito-LAR-GECO1.2 #
653 61245).

654

655 **Cloning of HA-ORP5, Mitofilin-GFP and GST- ORD5 (ORD ORP5)**

656 cDNAs of ORP5 (full-length), Mitoflin (full-length from FLAG-mitofilin (Ott et al., 2015))
657 and GST-ORD5 (corresponding to aa 265-703), were amplified by PCR. In all PCR
658 reactions, Herculase II fusion DNA polymerase (Agilent) was used.

659 Primers used were (coding sequence shown in lowercase):

660 5’ AgeI-HA-ORP5_Fw GGCGGC *ACCGGT* cgccacc ATGTACCCATACGATGTTCCA
661 GATTACGCT atgaaggaggaggccttcctc

662 3’ XhoI-STOP-ORP5_Rv GGC *CTCGAG* ctatttgaggatgtggttaatg

5' KpnI-Mitofilin_Fw AGACCCAAGCTT *GGTACC* atg

3' BamHI-GC-Mitofilin_Rv GTAATC *GGATTC* GC ctctggct

5' SalI-TC-ORD5_Fw GCACAG GTCGAC TC gagacccctggggccccggt

3' NotI-STOP-ORD5_Rv GCACA *GCGGCCGC* ctactgtggccggagggctggtcg

For the HA-ORP5 cloning the PCR product (carrying the HA tag at the N-terminus of ORP5) was ligated between AgeI and XhoI in the pEGFP-C1 vector (Clontech) and replacing the GFP- with the HA-tag. For the other clonings the PCR products were ligated between KpnI and BamHI for Mitofilin, and between SalI and NotI for ORD5, in the pEGFP-N1 vector (Clontech) to generate Mitofilin-EGFP or in the pGEX-6P-1 to generate GST-ORD5.

mRNA analyses by quantitative reverse transcriptase PCR (qPCR)

Total RNA was isolated from HeLa cells transfected with siRNAs for 48 hours as described above, by using a Purelink™ kit (Ambion/Thermo Scientific, Foster City, CA). The RNA (0.5 μg per specimen) was reverse transcribed with a SuperScript VILO™ cDNA synthesis kit (Invitrogen/Thermo Scientific, Carlsbad, CA) according to the manufacturer's protocol. Quantification of the mRNAs of interest was carried out on a Roche Lightcycler™ 480 II instrument by using SYBR-Green I Master mix (Roche, Basel, Switzerland) and primers specified in Table SX. Succinate dehydrogenase complex. subunit A, the mRNA of which remained markedly stable under the present conditions, was employed as a reference housekeeping mRNA. Relative mRNA levels were calculated by using the $-\Delta\Delta$Ct method.

Sequences of the primers used for qPCR:

mRNA	Sequence 5'-3'
SDHA* (housekeeping)	Fw: CATGCTGCCGTGTTCCGTGTGGG

	Rv: GGACAGGGTGTGCTTCCTCCAGTGCTCC
ORP5	Fw: GTGCCGCTGGAGGAGCAGAC
	Rv: AGGGGCTGTGGTCCTCGTATC
SAMM50	Fw: CAAGTGGACCTGATTTTGGAGG
	Rv: AGACGGAGCAATTTTTCACGG
Mitofilin	Fw: GTTGTATCTCAGTATCATGAGCTGG
	Rv: GTTCAGCTGATCAATACGACGA

*succinate dehydrogenase complex, subunit A

Antibodies, dyes and reagents list

Primary antibodies used in this study were:

	Antibody	Company & Reference
WB	IP3R-3	BD Transduction Laboratories, 610312
WB/IF/DUO	ORP5	SIGMA, HPA038712
WB	ORP5	SIGMA, HPA058727
WB	beta-Actin	Abcam, ab8226
DUO/IF	ORP8	Santa Cruz,
WB/IF/DUO	ORP8	GeneTex, GTX121273
IF, WB,DUO	SAMM50	SIGMA, HPA034537
WB	Mitofilin	Proteintech, 10179-1-AP
WB	PDI	GeneTex, GTX30716
WB	VAPB	SIGMA, HPA013144
WB	PSS1 (PTDSS1)	SIGMA, HPA016852
WB	PISD	SIGMA,HPA031090
IF, WB	GFP	Roche, 11814460001
IEM	GFP	Life technologies, A11122
IEM	PDI	Genetex, GTX30716

IF	HA	SIGMA, H3663
IF	FLAG M2	SIGMA, F1804
IF	MitoTracker® Red CMXRos	M7512, Invitrogen
IF	MitoTracker® Deep Red FM	M22426, Invitrogen

690

691 **Western blot**

692 For immunoblotting, cells were resuspended in lysis buffer [50 mM Tris, 150 mM
693 NaCl, 1% Triton X-100, 10 mM EDTA, pH 7.2, and protease inhibitor cocktail (Roche)].
694 Cell lysates were then centrifuged at 21 000 g for 20 min at 4°C. The supernatants
695 were boiled in reducing SDS sample buffer and proteins were separated using 10%
696 SDS-PAGE and immunoblot was carried using standard methods.

697 For Western blot quantification, bands of protein of interest were detected using
698 ChemiDoc™ Imaging Systems (Life Science Research, Bio-Rad) and analyzed using
699 Image Lab™ Software. All data are presented as mean ±SEM of three experimental
700 replicates.

701

702 **Immunoprecipitation of ORPs**

703 HeLa cells transfected with EGFP-tagged ORPs were washed in cold PBS and
704 lysed on ice in lysis buffer [50 mM Tris, 120 mM NaCl, 40 mM Hepes, 0.5% digitonin,
705 0.5% CHAPS, pH 7.36, and protease inhibitor cocktail (Roche). Cell lysates were then
706 centrifuged at 21 000 g for 20 min at 4°C. Supernatants were then incubated with
707 Chromotek GFP-trap agarose beads (Allele Biotech) for 1 hour at 4°C under rotation.
708 Subsequently beads were washed in 0.1 M phosphate buffer. After extensive washes
709 in cold lysis buffer, immunoprecipitated proteins bound to the beads were processed
710 for Mass Spectrometry analysis (see below) or incubated in sample buffer (containing

2% SDS) and then boiled for 1 min. In the latter case immunoprecipitates were loaded and separated in 10% SDS–PAGE gel and immunoblotting was carried out.

Cell fractionation

HeLa cells (100x10^6 cells) were harvested 48 hours after transfection with siRNA oligos and washed with PBS by centrifugation at 600 g for 5 min. The cell pellet was resuspended in starting buffer (225 mM mannitol, 75 mM sucrose and 30 mM Tris-HCl pH 7.4) and homogenized using a Tissue Grinder Dura-Grind®, Stainless Steel, Dounce (Wheaton). The homogenate was centrifuged three times at 600 g for 5 min to remove nuclei and unbroken cells. The crude mitochondria was pelleted by centrifugation at 10 000 g for 10 min. To separate MAM and pure mitochondria fractions, the pellet was resuspended in MRB buffer (250 mM mannitol, 5 mM HEPES and 0.5 mM EGTA, pH 7.4) and layered on top of different concentrations of Percoll gradient (225 mM mannitol, 25 mM HEPES, 1 mM EGTA pH 7.4 and 30% or 15% Percoll). After centrifugation at 95 000 g for 30 min, two dense bands containing either the pure mitochondria or MAM fraction were recovered and washed twice with MRB buffer by centrifugation at 6300 g for 10 min to remove residual Percoll and residual contamination. MAM was pelleted by centrifugation at 100 000 g for 1 hour. MAMs and pure mitochondria pellets were resuspended in Lysis Buffer (50 mM Tris, 150 mM NaCl, 1% Triton X-100, 10 mM EDTA, pH 7.2, and protease inhibitor cocktail) and protein concentrations were determined by Bradford assay. Equal amount of proteins were loaded on 4-20% gradient SDS-PAGE gels (Biorad) and immunoblotting was carried out. Pure mitochondria were processed for MS-lipidomic analysis (see below).

Mass spectrometry-proteomic analysis

Mass Spectrometry (MS) analysis was carried out by the proteomics/mass spectrometry platform in IJM (http://www.ijm.fr/plateformes/spectrometrie-de-masse). Briefly, after washes with binding buffer, immunoprecipitations beads were rinsed with 100 µl of NH4HCO3 25 mmol/l. Proteins on beads were digested overnight at 37°C by sequencing grade trypsin (12.5 µg/ml; Promega Madison, Wi, USA) in 20 µl of NH4HCO3 25 mmol/l. Digests were analysed by an Orbitrap Fusion (Thermo Fisher Scientific, San Jose, CA) equipped with a Thermo Scientific EASY-Spray nanoelectrospray ion source and coupled to an Easy nano-LC Proxeon 1000 system (Thermo Fisher Scientific, San Jose, CA). MS/MS data were processed with Proteome Discoverer 1.4 software (Thermo Fisher scientific, San Jose, CA) coupled to an in house Mascot search server (Matrix Science, Boston, MA; version 2.4.2). MS/MS datas were searched against SwissProt databases with Homo sapiens taxonomy. The Mascot score for a protein is the summed score for the individual peptides, e.g. peptide masses and peptide fragment ion masses, for all peptides matching a given protein. For a positive protein identification, the mascot score has to be above the 95% confidence level. In Mascot, the ions score for an MS/MS match is based on the calculated probability, P, that the observed match between the experimental data and the database sequence is a random event. The reported score is $-10\mathrm{Log}_{10}(P)$. A score of 200 indicates a probability of 10^{-20}. Scores greater than 70 are significant, while scores lower than 40 should not be considered or carefully validated at MS/MS level (source: http://www.matrixscience.com/help/interpretation_help.html). We thus set up a Mascot score threshold of 50.

Fluorescence Microscopy

Immunofluorescence and Confocal Microscopy

761 HeLa cells were seeded on 13 mm glass bottom coverslips (Agar Scientific).
762 Immunofluorescence was carried out one day after transfection. Transfected cells
763 were fixed with 4% PFA/PBS for 15 min at room temperature, washed in PBS and
764 incubated with 50 mM NH4Cl/PBS for 15 min at room temperature. After washing with
765 PBS and blocking buffer (1% BSA/ 0.1% Saponin in PBS), cells were incubated with
766 primary antibodies diluted in blocking buffer for 1 hour at room temperature and then
767 with fluorescently-labeled secondary antibodies. After washing with blocking buffer and
768 then PBS, coverslips were mounted on microscopy slides and images were acquired
769 on Confocal inverted microscope SP8-X (DMI 6000 Leica). Optical sections were
770 acquired with a Plan Apo 63x oil immersion objective (N.A. 1.4, Leica) using the LAS-
771 X software. Fluorescence was excited using either a 405nm laser diode or a white light
772 laser, and later collected after adjusting the spectral windows with GaAsP PMTs or
773 Hybrid detectors. Images from a mid-focal plane are shown. Images were processed
774 and fluorescence was analysed off line using Image J.

775 ***Quantifications***

776 For co-localization analysis of fluorescent signals, the acquired images were
777 processed using the JACoP plugin in ImageJ to assess the Pearson's correlation
778 coefficient. The obtained values, ranging from 0 to 1 (1=max correlation), indicated the
779 association between the signals analysed.

780

781 **Electron Microscopy Analysis**

782 ***Conventional EM***

783 For conventional EM, cells grown on 13 mm glass bottom coverslips (Agar
784 Scientific) were fixed with 2.5% glutaraldehyde and 2% PFA in 0.1 M cacodylate,
785 0.05% $CaCl_2$ buffer for 24 hours. After several washes with 0.1 M cacodylate buffer,

786 the cells were postfixed with 1% OsO_4, 1.5% potassium ferricyanide in 0.1M
787 Cacodylate for 1 hour. After several washes with 0.1 M cacodylate buffer and H_2O, the
788 cells were stained with 0.5% uranyl acetate for 24 hours. After several washes with
789 H_2O, the cells were dehydrated in ethanol and embedded in Epon while on the
790 coverslips. Ultrathin sections were prepared, counterstained with uranyl acetate and
791 observed under a MET JEOL 1400 equipped with a Orius High speed (Gatan) camera.

792 ***HRP Detection***

793 HeLa cells expressing HRP-KDEL were fixed on coverslips with 1.3%
794 glutaraldehyde in 0.1 M cacodylate buffer, washed in 0.1 M ammonium phosphate [pH
795 7.4] buffer for 1 hour and HRP was visualized with 0.5 mg/ml DAB and 0.005% H_2O_2
796 in 0.1 M Ammonium Phosphate [pH 7.4] buffer. Development of HRP (DAB dark
797 reaction product) took between 5 min to 20 min and was stopped by extensive washes
798 with cold water. Cells were postfixed in 2% OsO_4+1% $K_3Fe(CN)_6$ in 0.1 M cacodylate
799 buffer at 4°C for 1 hour, washed in cold water and then contrasted in 0.5% uranyl
800 acetate for 2 hours at 4°C, dehydrated in an ethanol series and embedded in epon as
801 for conventional EM. Ultrathin sections were counterstained with 2% uranyl acetate
802 and observed under a FEI Tecnai 12 microscope equipped with a CCD (SiS 1kx1k
803 keenView) camera.

804 ***Immunogold labelling***

805 HeLa cells were fixed with a mixture of 2%PFA and 0.125% glutaraldehyde in
806 0.1 M phosphate buffer [pH 7.4] for 2 hours, and processed for ultracryomicrotomy as
807 described previously (Slot & Geuze, 2007). Ultrathin cryosections were single- or
808 double-immunogold-labeled with antibodies and protein A coupled to 10 or 15 nm gold
809 (CMC, UMC Utrecht, The Netherlands), as indicated in the legends to the figures.

Immunogold-labeled cryosections were observed under a FEI Tecnai 12 microscope equipped with a CCD (SiS 1kx1k keenView) camera.

Quantifications

For the quantification of the number of cristae junction in Epon sections, about 200 mitochondria were analyzed in randomly selected cell profiles and cristae junctions were counted in each of the mitochondria profile and reported as number of cristae/mitochondria profile. All data are presented as mean ±SEM of three experimental replicates.

For the quantification of ER-mitochondria contact sites in HRP-stained Epon sections, the total circumference of each mitochondria and the length of the multiple HRP-positive ER segments closely associated (<30 nm) with them were measured by iTEM software (Olympus) on acquired micrographs of HeLa cells for each of 20-30 cell profiles, as indicated in the figure legends. Cells were randomly selected for analysis without prior knowledge of transfected plasmid or siRNA. All data are presented as mean (%) ±SEM of three experimental replicates.

For the quantification of immunogold labeling on ultrathin cryosections, 150 gold particles were counted on acquired micrographs of randomly selected cell profiles at specific ranges of distance from CJ (0-50, 50-100, 100-150, 150-200 nm) in each of three experiments. All data are presented as mean (%) ±SEM of three technical replicates.

***In situ* proximity ligation assay (PLA)**

The protein-protein interactions in fixed HeLa cells were assessed using *in situ* PLA (Duolink®SIGMA) according with the manufacturer's instructions. Briefly, HeLa cells seeded on glass coverslips were incubated with MitoTracker Red (1 μM in DMEM,

mitochondrial marker) for 30 min at 37°C or co-transfected with PHPLCd-RFP (plasma membrane marker) plus Mito-BFP (mitochondrial marker). Cells were thereafter fixed with 4% PFA for 30 minutes at room temperature and incubated with primary antibodies, monoclonal mouse anti-human ORP8 (1:150) polyclonal rabbit plus anti-human ORP5 (1:200, SIGMA), or monoclonal mouse anti-human ORP8 (1:150) plus polyclonal rabbit anti-human SAM50 (1:250, SIGMA), in blocking solution (1% BSA, w/v 0.01% saponin, w/v, in PBS) for 1h at room temperature. PLUS and MINUS PLA probes (anti-murine and anti-rabbit IgG antibodies conjugated with oligonucleotides, 1:5 in blocking solution) were then incubated with the samples for 1h at 37°C. Coverslips were thereafter washed in 1x wash buffer A and incubated with ligation solution (5x Duolink® Ligation buffer 1:5, ligase 1:40 in high purity water) for 30 min at 37°C. After the ligation step, cell samples were washed in 1x wash buffer A and incubated with the polymerase solution (5x Amplification buffer 1:5, polymerase 1:80 in high purity water) for 1h40min at 37°C. Polymerase solution was washed out from the coverslips with 1x wash buffer B and 0.01x wash buffer B. Vectashield Mounting Medium with or without DAPI (Vector Laboratories) was used for mounting.

Quantification of PLA

The number and the distance of PLA dots to mitochondria and to the plasma membrane were assessed using the Imaris software (v 9.3, Bitplane). Briefly, segmented 3D images (PLA foci identified as “spots”, mitochondria identified as “surfaces”, and plasma membrane represented as “cell” were generated from confocal Z-stack images and the shortest distance between each spot center and the nearest point of the surface or cell object was calculated based on a 3D distance map. Spots objects (PLA dots) with a distance smaller than 380nm from surfaces (mitochondria) and cell (plasma membrane) objects were considered at a close proximity of these

objects. The threshold of 380 nm was used as an estimation of the PLA reaction precision including both primary and secondary antibodies (30nm) plus half the FWHM of the PLA amplification signals (350nm).

Mass Spectrometry-lipidomic analysis

700 µl of homogenized cells were mixed with 800 µl 1 N HCl:CH_3OH 1:8 (v/v), 900 µl $CHCl_3$ and 200 µg/ml of the antioxidant 2,6-di-tert-butyl-4-methylphenol (BHT; Sigma Aldrich). The organic fraction was evaporated using a Savant Speedvac spd111v (Thermo Fisher Scientific). Lipid pellets were reconstituted in running solution (CH_3OH:$CHCl_3$:NH_4OH; 90:10:1.25; v/v/v). Phospholipid species were analyzed by electrospray ionization tandem mass spectrometry (ESI-MS/MS) on a hybrid triple quadrupole/linear ion trap mass spectrometer (4000 QTRAP system; Applied Biosystems SCIEX) equipped with a TriVersa NanoMate (Advion Biosciences) robotic nanosource. Phospholipid profiling was executed by (positive or negative) precursor ion or neutral loss scanning at a collision energy of 35 eV for neutral loss 141 (phosphatidylethanolamine (PE)). Phospholipid quantification was performed by multiple reaction monitoring (MRM), the transitions being based on the neutral losses or the typical product ions as described above. The MRM dwell time was set to 100 ms and typically the signal was averaged over 20 cycles. Lipid standards used were PE25:0 and PE43:6 (Avanti Polar Lipids). The data were corrected for isotope effects as described by (Liebisch, Lieser et al., 2004).

Lipid Transfer assay

ORP5 and ORP8 ORD domain purification

884 Escherichia coli BL21DE3 RILP (Invitrogen) cells were transformed with plasmids
885 encoding for GST tagged ORP5 or ORP8 ORD domains following the manufacturer's
886 instruction. Bacteria were then grown overnight at 37°C and used to inoculate a large-
887 scale volume (1L). When the OD_{600} reached 0.4, cultures were cooled down and
888 incubated at 18°C until they reached O_{D600} = 0.65. Cells were induced by addition
889 of isopropyl β-D-1-thiogalactopyranoside to a final concentration of 0.1 mM and
890 incubated overnight at 18°C before harvesting. Cells were resuspended in 35 mL
891 binding buffer (1X PBS, 1 mM EDTA, 1 mM DTT, Protease inhibitor) then 250 units of
892 benzonase nuclease (Sigma) were added to the resuspension. Cells were lysed by
893 sonication and the supernatant was recover after 20 min centrifugation at 184 000g
894 and 4°C. Supernatant containing GST tagged proteins was incubated with 2 mL of
895 Glutathione Sepharose 4 fast flow for 1 hour at 4°C under nutation. Beads were
896 washed using a series of wash buffers: 1st (1X PBS, 1 mM EDTA, 1 mM DTT), 2nd
897 HSP-removal buffer (50 mM Tris pH 7.5, 50 mM KCl, 20 mM $MgCl_2$, 5 mM ATP) then
898 cleavage buffer (50 mM Tris pH 7.5, 150 mM NaCl, 1 mM EDTA, 1 mM DTT). Cleavage
899 of the GST tag was realized overnight at 4°C using Prescission protease. Untagged
900 proteins were eluted with cleavage buffer, flash frozen and stored at -80°C until lipid
901 transfer assay was performed.

902 ***Lipids***

903 1-palmitoyl-2-oleoyl-sn-glycero-3-phosphocholine (POPC), 1,2-dioleoyl-sn-
904 glycero-3-phosphoethanolamine-N-(cap biotinyl) (Biotinyl Cap PE), 1-palmitoyl-2-
905 (dipyrrometheneboron difluoride)undecanoyl-sn-glycero-3-phosphoethanolamine
906 (TopFluor-PE), 1-palmitoyl-2-(dipyrrometheneboron difluoride)undecanoyl-sn-glycero-
907 3-phospho-L-serine (TopFluor-PS), 1-palmitoyl-2-(dipyrrometheneboron

908 difluoride)undecanoyl-sn-glycero-3-phosphocholine (TopFluor-PC) were purchased
909 from Avanti Polar Lipids as chloroform solutions.

910 ***Liposome preparation***

911 1 µmol of the appropriate lipid mixtures in chloroform solution was dried in a glass
912 tube for 10 min under a gentle stream of argon, and then for 1 hour under vacuum.
913 The dried lipid films were resuspended in 1 mL of buffer H (25 mM HEPES/KOH, pH
914 7.7; 150 mM KCl; 10%(v/v) Glycerol) by vigorously vortexing for 30 min at room
915 temperature. Unilamellar liposomes were produced by seven freeze-thaw cycles (30
916 sec in liquid nitrogen followed by 5 min in a 37°C water bath) and extrusion (at least
917 21 times) through a polycarbonate filter with 100 nm pore size (polycarbonate
918 membranes from Avanti Polar Lipids). The liposomes were then stored on ice.

919 ***Lipid Transfer assay in vitro***

920 The lipid transfer assays were realized with liposomes prepared as described
921 above. The donor liposomes contained 1% mol TopFluor lipids (-PS, -PC or -PE) and
922 2% mol Biotinyl Cap PE. The acceptor liposomes contained only POPC. For each
923 reaction, 25 µL of streptavidin-coated magnetic beads (DynabeadsMyOne Streptavidin
924 T1, Invitrogen) were washed in buffer H and mixed with 25 µL of 1 mM donor
925 liposomes. The mixture was incubated for 1 hour at 25°C with intermittent gentle
926 mixing. Bead-bound donor liposomes were then washed, resuspended in 25 µL and
927 mixed with 25 µL of 1 mM acceptor liposomes and 50 µL of buffer H or protein (0.3 µM
928 protein and 2.5 µM TopFluor lipids in the reaction solution). The mixture was incubated
929 at 37°C for 1 hour with intermittent gentle mixing. Supernatant containing acceptor
930 liposomes was recovered after binding of bead-bound donor liposomes to a magnetic
931 rack. TopFluor fluorescence of acceptor and donor liposomes was measured (after
932 solubilization with 0.4% (w/v) n-dodecyl-β-D-maltoside, DDM) in a SpectraMax M5

plate reader (Molecular Device) equilibrated to 30°C (excitation: 450 nm; emission: 510 nm; cutoff: 475 nm; low gain). The percentage of lipids transferred from donor to acceptor liposomes was determined using the following formula: $100*F_{acceptor}/(F_{acceptor}+F_{donor})$. To confirm that fluorescence was transferred to acceptor liposomes, a fraction of the reaction supernatant – which has not been solubilized with DDM – was floated on a Nycodenz density gradient. 50 µL of supernatant was mixed with 100 µL of buffer H and 150 µL of Nycodenz 80% in buffer H. The solution was transferred to a 0.8 mL Ultra-Clear centrifuge tube (Beckman Coulter) and overlaid with 250 µL of Nycodenz 30% in buffer H and 75 µL of buffer H. The tubes were centrifuged in a SW 55 Ti rotor (Beckman Coulter) at 246,000 g for 4 hours at 4 °C. 50 µL were collected from the top of the gradient and the fluorescence was measured.

Radiometric assay for the conversion of PS to PE *in situ*

Hela cells were seeded on 6-well plates and transfected for 48 hours with the non-targeting, ORP5 or ORP8-specific siRNAs specified above by using Oligofectamine (Thermo Fisher Scientific). The cells were then washed and shifted into Hanks balanced salt solution (Gibco) supplemented with a serine-free MEM amino acid mixture and MEM vitamins (Gibco), followed by 18 hours labeling with 2 µl/well L-[^{3}H(G)]serine (30.9 Ci/mmol, NET24800, Perkin-Elmer)(Fig. 1e). In parallel experiments (Fig. 1f) cells were starved in serum-free medium for 10 hours and then treated with 1mM β-chloro-L-alanine (SIGMA) for 2 hours or left in serum-free medium, followed by 1hr pulse with 15 µCi/ml of [^{3}H(G)]serine and 12 hours chase in serum-free DMEM. After the labeling (Fig. 1e) or the chase (Fig. 1f), the cells were scraped into 0.9 ml 2% NaCl per well, a 0.1 ml aliquot was withdrawn for protein analysis with the BCA assay (Thermo Fisher Scientific), and, after adding 50 nmol of

unlabeled PS as carrier, the remaining 0.8 ml was subjected to lipid extraction by an acid modification of the Folch method (Kim, Song et al., 2017). After drying, the lipids were resolved in 50 μl $CHCl_3$ and applied on Merck TLC Silica gel 60^{TM} plates, followed by separation by using $CHCl_3$-methanol-acetic acid-H2O (50:30:8:3.5) as solvent. The PS and PE spots identified from the mobility of standards run on the same plates were scraped into scintillation vials for analysis of [^{3}H] radioactivity. The DPM values were corrected for total cell protein, and the ratio of [^{3}H] in PE vs. PS calculated.

Mitochondrial respiration assay

Oxygen Consumption rate (OCR) was measured using the XF_p Extracellular Flux Analyzer (Seahorse Bioscience Inc.). HeLa cells were seeded on a 6-well plate 3 days before the Seahorse experiment and knockdown of the proteins of interest was realized 2 days before. The day after the knockdown, HeLa cells transfected with Ctrl, ORP5, or ORP8 siRNAs were plated in a Seahorse XFp 8-mini wells microplate. 20,000 HeLa cells were seeded in each well (except in the blank wells used for the background correction) in 180 μl of culture medium, and incubated overnight at 37℃ in 5% CO2. One day after, the culture medium was replaced with 180 μl of XF DMEM Medium Solution pH 7.4 and then the 8-mini wells microplate was moved in a 37°C non-CO2 incubator before measurement. OCR was determined before drug additions and after addition of Oligomycin (1.5 μM), Carbonyl cyanide 4-(trifluoromethoxy) phenylhydrazone (FCCP, 0.5 μM), and Rotenone/Antimycin A (0.5 μM) (purchased from Agilent). After each assay, all the raw OCR data were analyzed using WAVE software.

Statistical Analysis

Statistical analysis was performed with Microsoft Excel or GraphPad Prism 9.0. The data were presented as mean ± standard error of the mean (SEM). The n, indicated in the figures and figure legends, represent the total number of cells analyzed in three or more biological replicates, as stated in the figures legend. Statistical significance of two data sets were determined by unpaired student's *t*-test, with * $p<0.05$, *** $p<0.01$, ***$p<0.001$ and **** $p<0.0001$.

ACKNOWLEDGEMENTS

We thank Dr V. Kozjak-Pavlovic and P. Somerharju for kindly sharing reagents and advices with us. We also thank Dr. R. Legouis, Dr. Emmanuel Culetto for discussion and for critically reading the manuscript; Claire Boulogne, Sandrine Lécart and Remi Le Borgne for help and consultation with microscopy experiments; Valentin Guyard, Blandine Bourigault, Riikka Kosonen and Liisa Arala for technical assistance. The present work has benefited from Imagerie-Gif core facility supported by l'Agence Nationale de la Recherche (ANR-11-EQPX-0029/Morphoscope, ANR-10-INBS-04/FranceBioImaging; ANR-11-IDEX-0003-02/ Saclay Plant Sciences). For the Immuno-EM and HRP-KDEL EM analysis/quantifications we acknowledge the ImagoSeine facility, member of the France BioImaging infrastructure supported by grant ANR-10-INBS-04 from the French National Research Agency. We also thank Jean-Michel Camadro and Thibault Leger (IJM proteomics platform) for proteomics analysis. This work was supported by the ANR Jeune Chercheur (ANR0015TD), the ATIP-Avenir Program, the FSER (FRM n°206548) and the FVA (eOTP:669122 LS 212527) to F.G.; the Academy of Finland (grants 285223 and 322647), the Sigrid Juselius Foundation, the Finnish Foundation for Cardiovascular Research and the

Magnus Ehrnrooth Foundation to V.M.O.; the “Association Française contre les Myopathies” (AFM Research grant 20123) and the ITMO-Inserm Plan Cancer 2014-2019 to D.T.

AUTHOR CONTRIBUTIONS

FG conceived and supervised the work. VO designed and supervised the radiometric assays for PS-to-PE conversion and the expression analysis by RT-PCR. DT designed and supervised the *in vitro* lipid transfer assays. LR performed and analyzed the cell experiments including cell imaging and Seahorse analysis. VC performed and analyzed the cell experiments including immunofluorescence for endogenous proteins and Duolink. LR, AH, and FG performed and analyzed the EM experiments. CS participated to the setting up of the Seahorse experiments. CS, AH and DT performed and analyzed the *in vitro* lipid transfer assays. AA, EJ and AK performed and analyzed the radiometric assays for PS-to-PE conversion. EM, JD and JS performed MS-lipidomic analysis. RLB provided tools and techniques for Duolink imaging analysis. JN and NEK provided technical help in western blot analysis and generated some of the constructs for mammalian cell expression. LR, VC and FG wrote the manuscript and all authors commented on the manuscript.

CONFLICT OF INTERESTS

The authors declare that they have no competing interests.

DATA AVAILABILITY SECTION

This study includes no data deposited in external repositories.

REFERENCES

1035 Aaltonen MJ, Friedman JR, Osman C, Salin B, di Rago JP, Nunnari J, Langer T, Tatsuta T
1036 (2016) MICOS and phospholipid transfer by Ups2-Mdm35 organize membrane lipid
1037 synthesis in mitochondria. The Journal of cell biology 213: 525-34
1038 Chen H, Born E, Mathur SN, Field FJ (1993) Cholesterol and sphingomyelin syntheses are
1039 regulated independently in cultured human intestinal cells, CaCo-2: role of membrane
1040 cholesterol and sphingomyelin content. J Lipid Res 34: 2159-67
1041 Chung J, Torta F, Masai K, Lucast L, Czapla H, Tanner LB, Narayanaswamy P, Wenk MR,
1042 Nakatsu F, De Camilli P (2015) INTRACELLULAR TRANSPORT. PI4P/phosphatidylserine
1043 countertransport at ORP5- and ORP8-mediated ER-plasma membrane contacts. Science
1044 349: 428-32
1045 Ding C, Wu Z, Huang L, Wang Y, Xue J, Chen S, Deng Z, Wang L, Song Z, Chen S (2015)
1046 Mitofilin and CHCHD6 physically interact with Sam50 to sustain cristae structure. Sci
1047 Rep 5: 16064
1048 Friedman JR, Mourier A, Yamada J, McCaffery JM, Nunnari J (2015) MICOS coordinates
1049 with respiratory complexes and lipids to establish mitochondrial inner membrane
1050 architecture. eLife 4
1051 Gallo A, Danglot L, Giordano F, Hewlett B, Binz T, Vannier C, Galli T (2020) Role of the
1052 Sec22b-E-Syt complex in neurite growth and ramification. Journal of cell science 133
1053 Galmes R, Houcine A, van Vliet AR, Agostinis P, Jackson CL, Giordano F (2016)
1054 ORP5/ORP8 localize to endoplasmic reticulum-mitochondria contacts and are involved
1055 in mitochondrial function. EMBO reports 17: 800-10
1056 Ghai R, Du X, Wang H, Dong J, Ferguson C, Brown AJ, Parton RG, Wu JW, Yang H (2017)
1057 ORP5 and ORP8 bind phosphatidylinositol-4, 5-biphosphate (PtdIns(4,5)P 2) and
1058 regulate its level at the plasma membrane. Nature communications 8: 757
1059 Giordano F (2018) Non-vesicular lipid trafficking at the endoplasmic reticulum-
1060 mitochondria interface. Biochemical Society transactions 46: 437-452
1061 Giordano F, Saheki Y, Idevall-Hagren O, Colombo SF, Pirruccello M, Milosevic I, Gracheva
1062 EO, Bagriantsev SN, Borgese N, De Camilli P (2013) PI(4,5)P2-Dependent and Ca(2+)-
1063 Regulated ER-PM Interactions Mediated by the Extended Synaptotagmins. Cell 153:
1064 1494-509
1065 Guarani V, McNeill EM, Paulo JA, Huttlin EL, Frohlich F, Gygi SP, Van Vactor D, Harper JW
1066 (2015) QIL1 is a novel mitochondrial protein required for MICOS complex stability and
1067 cristae morphology. eLife 4
1068 Hanada K, Nishijima M, Kiso M, Hasegawa A, Fujita S, Ogawa T, Akamatsu Y (1992)
1069 Sphingolipids are essential for the growth of Chinese hamster ovary cells. Restoration of
1070 the growth of a mutant defective in sphingoid base biosynthesis by exogenous
1071 sphingolipids. The Journal of biological chemistry 267: 23527-33
1072 Harner M, Korner C, Walther D, Mokranjac D, Kaesmacher J, Welsch U, Griffith J, Mann M,
1073 Reggiori F, Neupert W (2011) The mitochondrial contact site complex, a determinant of
1074 mitochondrial architecture. The EMBO journal 30: 4356-70
1075 Heikinheimo L, Somerharju P (1998) Preferential decarboxylation of hydrophilic
1076 phosphatidylserine species in cultured cells. Implications on the mechanism of transport
1077 to mitochondria and cellular aminophospholipid species compositions. The Journal of
1078 biological chemistry 273: 3327-35
1079 Herrera-Cruz MS, Simmen T (2017) Of yeast, mice and men: MAMs come in two flavors.
1080 Biol Direct 12: 3
1081 Hirabayashi Y, Kwon SK, Paek H, Pernice WM, Paul MA, Lee J, Erfani P, Raczkowski A,
1082 Petrey DS, Pon LA, Polleux F (2017) ER-mitochondria tethering by PDZD8 regulates
1083 Ca(2+) dynamics in mammalian neurons. Science 358: 623-630

1084 Hohr AIC, Lindau C, Wirth C, Qiu J, Stroud DA, Kutik S, Guiard B, Hunte C, Becker T,
1085 Pfanner N, Wiedemann N (2018) Membrane protein insertion through a mitochondrial
1086 beta-barrel gate. Science 359
1087 Huynen MA, Muhlmeister M, Gotthardt K, Guerrero-Castillo S, Brandt U (2016) Evolution
1088 and structural organization of the mitochondrial contact site (MICOS) complex and the
1089 mitochondrial intermembrane space bridging (MIB) complex. Biochimica et biophysica
1090 acta 1863: 91-101
1091 John GB, Shang Y, Li L, Renken C, Mannella CA, Selker JM, Rangell L, Bennett MJ, Zha J
1092 (2005) The mitochondrial inner membrane protein mitofilin controls cristae
1093 morphology. Molecular biology of the cell 16: 1543-54
1094 Joshi AS, Thompson MN, Fei N, Huttemann M, Greenberg ML (2012) Cardiolipin and
1095 mitochondrial phosphatidylethanolamine have overlapping functions in mitochondrial
1096 fusion in Saccharomyces cerevisiae. The Journal of biological chemistry 287: 17589-97
1097 Kim SH, Song HE, Kim SJ, Woo DC, Chang S, Choi WG, Kim MJ, Back SH, Yoo HJ (2017)
1098 Quantitative structural characterization of phosphatidylinositol phosphates from
1099 biological samples. J Lipid Res 58: 469-478
1100 Kopec KO, Alva V, Lupas AN (2010) Homology of SMP domains to the TULIP superfamily
1101 of lipid-binding proteins provides a structural basis for lipid exchange between ER and
1102 mitochondria. Bioinformatics 26: 1927-31
1103 Kornmann B, Currie E, Collins SR, Schuldiner M, Nunnari J, Weissman JS, Walter P (2009)
1104 An ER-mitochondria tethering complex revealed by a synthetic biology screen. Science
1105 325: 477-81
1106 Kozjak V, Wiedemann N, Milenkovic D, Lohaus C, Meyer HE, Guiard B, Meisinger C,
1107 Pfanner N (2003) An essential role of Sam50 in the protein sorting and assembly
1108 machinery of the mitochondrial outer membrane. The Journal of biological chemistry
1109 278: 48520-3
1110 Kozjak-Pavlovic V, Ross K, Benlasfer N, Kimmig S, Karlas A, Rudel T (2007) Conserved
1111 roles of Sam50 and metaxins in VDAC biogenesis. EMBO reports 8: 576-82
1112 Kumar N, Leonzino M, Hancock-Cerutti W, Horenkamp FA, Li P, Lees JA, Wheeler H,
1113 Reinisch KM, De Camilli P (2018) VPS13A and VPS13C are lipid transport proteins
1114 differentially localized at ER contact sites. The Journal of cell biology 217: 3625-3639
1115 Lang A, John Peter AT, Kornmann B (2015) ER-mitochondria contact sites in yeast:
1116 beyond the myths of ERMES. Current opinion in cell biology 35: 7-12
1117 Liebisch G, Lieser B, Rathenberg J, Drobnik W, Schmitz G (2004) High-throughput
1118 quantification of phosphatidylcholine and sphingomyelin by electrospray ionization
1119 tandem mass spectrometry coupled with isotope correction algorithm. Biochimica et
1120 biophysica acta 1686: 108-17
1121 Maeda K, Anand K, Chiapparino A, Kumar A, Poletto M, Kaksonen M, Gavin AC (2013)
1122 Interactome map uncovers phosphatidylserine transport by oxysterol-binding proteins.
1123 Nature 501: 257-61
1124 Ott C, Dorsch E, Fraunholz M, Straub S, Kozjak-Pavlovic V (2015) Detailed analysis of the
1125 human mitochondrial contact site complex indicate a hierarchy of subunits. PloS one 10:
1126 e0120213
1127 Reinisch KM, De Camilli P (2016) SMP-domain proteins at membrane contact sites:
1128 Structure and function. Biochimica et biophysica acta 1861: 924-927
1129 Schikorski T, Young SM, Jr., Hu Y (2007) Horseradish peroxidase cDNA as a marker for
1130 electron microscopy in neurons. Journal of neuroscience methods 165: 210-5
1131 Scorrano L, De Matteis MA, Emr S, Giordano F, Hajnoczky G, Kornmann B, Lackner LL,
1132 Levine TP, Pellegrini L, Reinisch K, Rizzuto R, Simmen T, Stenmark H, Ungermann C,

Schuldiner M (2019) Coming together to define membrane contact sites. Nature communications 10: 1287

Shiao YJ, Lupo G, Vance JE (1995) Evidence that phosphatidylserine is imported into mitochondria via a mitochondria-associated membrane and that the majority of mitochondrial phosphatidylethanolamine is derived from decarboxylation of phosphatidylserine. The Journal of biological chemistry 270: 11190-8

Shibata Y, Voss C, Rist JM, Hu J, Rapoport TA, Prinz WA, Voeltz GK (2008) The reticulon and DP1/Yop1p proteins form immobile oligomers in the tubular endoplasmic reticulum. The Journal of biological chemistry 283: 18892-904

Slot JW, Geuze HJ (2007) Cryosectioning and immunolabeling. Nature protocols 2: 2480-91

Steenbergen R, Nanowski TS, Beigneux A, Kulinski A, Young SG, Vance JE (2005) Disruption of the phosphatidylserine decarboxylase gene in mice causes embryonic lethality and mitochondrial defects. The Journal of biological chemistry 280: 40032-40

Stoica R, De Vos KJ, Paillusson S, Mueller S, Sancho RM, Lau KF, Vizcay-Barrena G, Lin WL, Xu YF, Lewis J, Dickson DW, Petrucelli L, Mitchell JC, Shaw CE, Miller CC (2014) ER-mitochondria associations are regulated by the VAPB-PTPIP51 interaction and are disrupted by ALS/FTD-associated TDP-43. Nature communications 5: 3996

Tamura Y, Endo T (2017) Role of Intra- and Inter-mitochondrial Membrane Contact Sites in Yeast Phospholipid Biogenesis. Advances in experimental medicine and biology 997: 121-133

Tasseva G, Bai HD, Davidescu M, Haromy A, Michelakis E, Vance JE (2013) Phosphatidylethanolamine deficiency in Mammalian mitochondria impairs oxidative phosphorylation and alters mitochondrial morphology. The Journal of biological chemistry 288: 4158-73

Tatsuta T, Scharwey M, Langer T (2014) Mitochondrial lipid trafficking. Trends in cell biology 24: 44-52

Vance JE (1990) Phospholipid synthesis in a membrane fraction associated with mitochondria. The Journal of biological chemistry 265: 7248-56

Vance JE (2014) MAM (mitochondria-associated membranes) in mammalian cells: lipids and beyond. Biochimica et biophysica acta 1841: 595-609

Vance JE, Tasseva G (2013) Formation and function of phosphatidylserine and phosphatidylethanolamine in mammalian cells. Biochimica et biophysica acta 1831: 543-54

Wang H, Ma Q, Qi Y, Dong J, Du X, Rae J, Wang J, Wu WF, Brown AJ, Parton RG, Wu JW, Yang H (2019) ORP2 Delivers Cholesterol to the Plasma Membrane in Exchange for Phosphatidylinositol 4, 5-Bisphosphate (PI(4,5)P2). Mol Cell 73: 458-473 e7

Wideman JG (2015) The ubiquitous and ancient ER membrane protein complex (EMC): tether or not? F1000Res 4: 624

Wideman JG, Balacco DL, Fieblinger T, Richards TA (2018) PDZD8 is not the 'functional ortholog' of Mmm1, it is a paralog. F1000Res 7: 1088

Wollweber F, von der Malsburg K, van der Laan M (2017) Mitochondrial contact site and cristae organizing system: A central player in membrane shaping and crosstalk. Biochimica et biophysica acta 1864: 1481-1489

Yeo HK, Park TH, Kim HY, Jang H, Lee J, Hwang GS, Ryu SE, Park SH, Song HK, Ban HS, Yoon HJ, Lee BI (2021) Phospholipid transfer function of PTPIP51 at mitochondria-associated ER membranes. EMBO reports 22: e51323

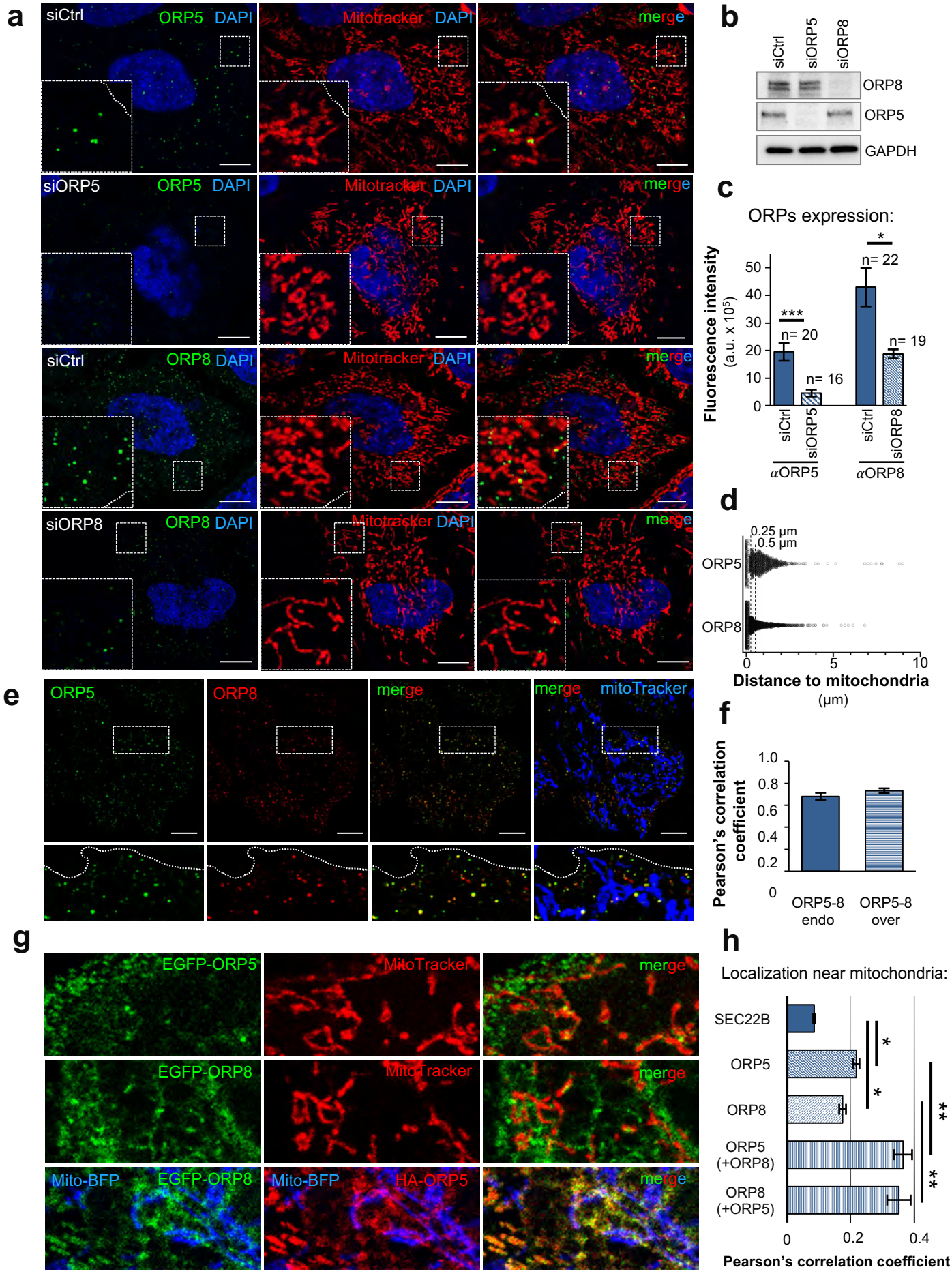
a
siCtrl
ORP5 DAPI
Mitotracker DAPI
merge
siORP5
ORP5 DAPI
Mitotracker DAPI
merge
siCtrl
ORP8 DAPI
Mitotracker DAPI
merge
siORP8
ORP8 DAPI
Mitotracker DAPI
merge
b
siCtrl
siORP5
siORP8
ORP8
ORP5
GAPDH
c
ORPs expression:
Fluorescence intensity
(a.u. x 10^5)
50
40
30
20
10
0
***
n= 20
n= 16
*
n= 22
n= 19
siCtrl
siORP5
siCtrl
siORP8
αORP5
αORP8
d
0.25 µm
0.5 µm
ORP5
ORP8
0
5
10
Distance to mitochondria
(µm)
e
ORP5
ORP8
merge
merge mitoTracker
f
Pearson's correlation coefficient
1.0
0.8
0.6
0.4
0.2
0
ORP5-8 endo
ORP5-8 over
g
EGFP-ORP5
MitoTracker
merge
EGFP-ORP8
MitoTracker
merge
Mito-BFP
EGFP-ORP8
Mito-BFP
HA-ORP5
merge
h
Localization near mitochondria:
SEC22B
ORP5
ORP8
ORP5 (+ORP8)
ORP8 (+ORP5)
*
*
**
**
0
0.2
0.4
Pearson's correlation coefficient

Figure 1

Figure 1. Endogenous and co-overexpressed ORP5 and ORP8 co-localize at ER-mitochondria contact sites. (a) Confocal images of Ctrl, ORP5 and ORP8 knockdown HeLa cells were immunostained using anti-ORP5 or ORP8 antibodies (green), and treated with MitoTracker to label mitochondria (red) and DAPI to stain the nuclei (blue). Images are presented as individual layers. Insets show magnifications of the boxed regions. Note the close association of endogenous ORP5 and ORP8 to mitochondria. Scale bar, 10 μm. (b) WB analysis showing ORP5, ORP8 and GAPDH levels in protein lysates from Ctrl, ORP5 and ORP8 knockdown HeLa cells. (c) Quantification of ORP5 and ORP8 fluorescent intensity in Ctrl, ORP5 and ORP8 knockdown cells. Mean of fluorescent intensities in arbitrary units (a.u. $x10^5$). Error bars denote ± standard error of the mean (SEM). Number of cells given above bars. Statistical analysis: P values were determined by unpaired student's *t*-test, *P<0.05, ***P<0.001. (d) Distribution of ORP5 and ORP8 IF staining (spots) in relation to their distance (in μm) to mitochondria indicating that part of the endogenous ORP5 and ORP8 in the cell is detected in close proximity to mitochondria (<0.5 μm). (e) Confocal images of a HeLa cell immunostained using anti-ORP5 (green) or ORP8 (red) antibodies and MitoTracker (blue). Images are presented as individual layers. Insets show magnifications of the boxed regions. Scale bar, 10 μm. (f) Quantification of the co-localization (Pearson's factor) of ORP5-ORP8 in endogenous (ORP5-8 end) and co-overexpression (ORP5-8 over) conditions. Bars indicate mean values ± SEM. Number of cell analyzed: ORP5-8 end (n=15), ORP5-8 over (n=14). (g**)** Confocal micrograph of a region of HeLa cell (zoomed from Fig EV1a) transfected with EGFP-ORP5 (green), EGFP-ORP8 (green) or EGFP-ORP8 (green) + HA-ORP5 (anti-HA, red), and with Mito-BFP (blue). (h) Quantifications of the association to mitochondria (Pearson's factor) of the indicated EGFP-tagged constructs. Bars indicate mean values ± SEM of three independent experiments with 10 cells for sample analyzed in each experiment (n=30). Statistical analysis: unpaired Student's t-test comparing EGFP-ORP5 (ORP5) or EGFP-ORP8 (ORP8) to EGFP-Sec22b (SEC22b) and HA-ORP5 (+EGFP-ORP8) or EGFP-ORP8 (+HA-ORP5) to EGFP-ORP5 or EGFP-ORP8, respectively. *P<0.05, **P<0.01.

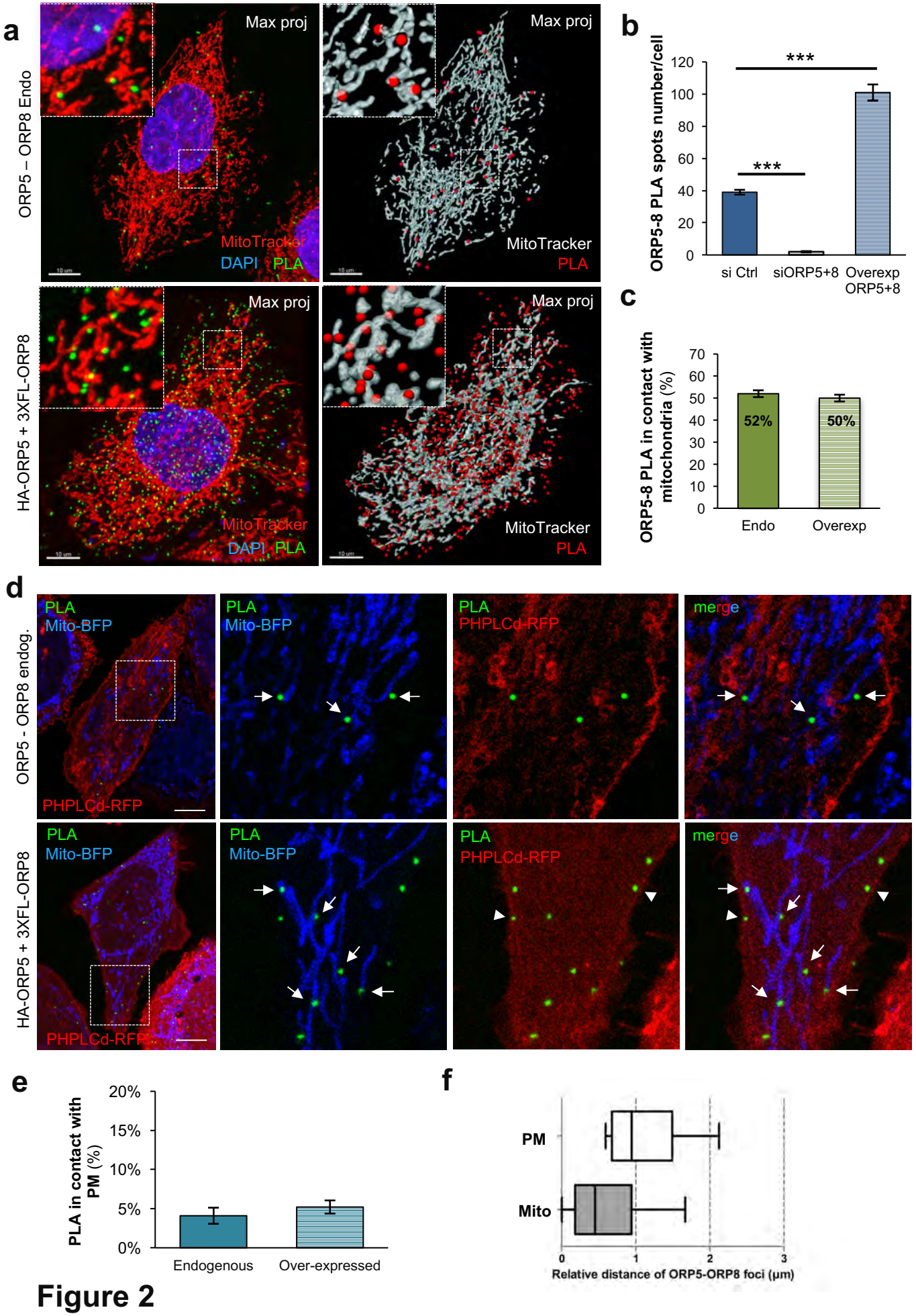
a
ORP5 – ORP8 Endo
Max proj
MitoTracker
DAPI PLA
Max proj
MitoTracker
PLA
HA-ORP5 + 3XFL-ORP8
Max proj
MitoTracker
DAPI PLA
Max proj
MitoTracker
PLA
b
ORP5-8 PLA spots number/cell
120
100
80
60
40
20
0
***
***
si Ctrl
siORP5+8
Overexp ORP5+8
c
ORP5-8 PLA in contact with mitochondria (%)
70
60
50
40
30
20
10
0
52%
50%
Endo
Overexp
d
ORP5 - ORP8 endog.
PLA
Mito-BFP
PHPLCd-RFP
PLA
Mito-BFP
PLA
PHPLCd-RFP
merge
HA-ORP5 + 3XFL-ORP8
PLA
Mito-BFP
PHPLCd-RFP
PLA
Mito-BFP
PLA
PHPLCd-RFP
merge
e
PLA in contact with PM (%)
20%
15%
10%
5%
0%
Endogenous
Over-expressed
f
PM
Mito
0
1
2
3
Relative distance of ORP5-ORP8 foci (µm)

Figure 2

Figure 2. The main localization of the endogenous ORP5-8 complex is ER-mitochondria contact sites. (a**)** Representative confocal images of ORP5-ORP8 interaction in HeLa cells detected by Duolink PLA (green spots) in endogenous (ORP5-ORP8 Endo) and overexpressing (HA-ORP5 + 3xFL-ORP8) conditions, and their respective 3D representation by Imaris. Images are presented as maximum projection of all layers. Insets show magnifications of the boxed regions. Scale bar, 10 µm. (b) Quantification of the number of ORP5-ORP8 PLA interactions in Control (siCtrl, n=39 cells), ORP5 and ORP8 knockdown (siORP5+8, n=38 cells), and in overexpression of ORP5 and ORP8 (Ovrexp ORP5+8, n=35 cells), showing that the downregulation or the upregulation of both ORP5 and ORP8, respectively, reduces and increases the number of interaction stablished between these two proteins. Statistical analysis: P values were determined by unpaired student's *t*-test, ***P<0,001. (c) Quantification of ORP5-ORP8 PLA interaction localized to ER-Mitochondria contact sites in control (Endo, n= 33) and HeLa cells overexpressing (HA-ORP5 + 3xFL-ORP8, n=27 cells) showing that about 50% of ORP5-ORP8 interactions occurs at MAM. (d) Representative confocal images of ORP5-ORP8 PLA interaction (green spots) detected in HeLa cells overexpressing PHPLCd-RFP, Mito-BFP (ORP5-ORP8 Endo), or in HeLa cells overexpressing PHPLCδ-RFP, Mito-BFP, ORP5 and ORP8 (HA-ORP5 + 3xFL-ORP8). Images are presented as individual layers. Scale bar, 10 µm. (e) Quantification of ORP5-ORP8 PLA signal localized to ER-plasma membrane contact sites indicate that about 5% of the total ORP5-ORP8 interactions occurs to these subdomains of the ER membranes, in both control (Endogenous, n=6 cells) and HeLa cells overexpressing ORP5 and ORP8 (Overexpressed, n=14 cells). (f) Box plot of ORP5-ORP8 endogenous PLA spots distance (in µm) to mitochondria and plasma membrane (box around median value, whiskers 10%-90%) evidencing that the majority of ORP5-ORP8 interactions were detected in a close proximity to mitochondria (<0.38 µm) and distant from the plasma membrane (≥0.38 µm).

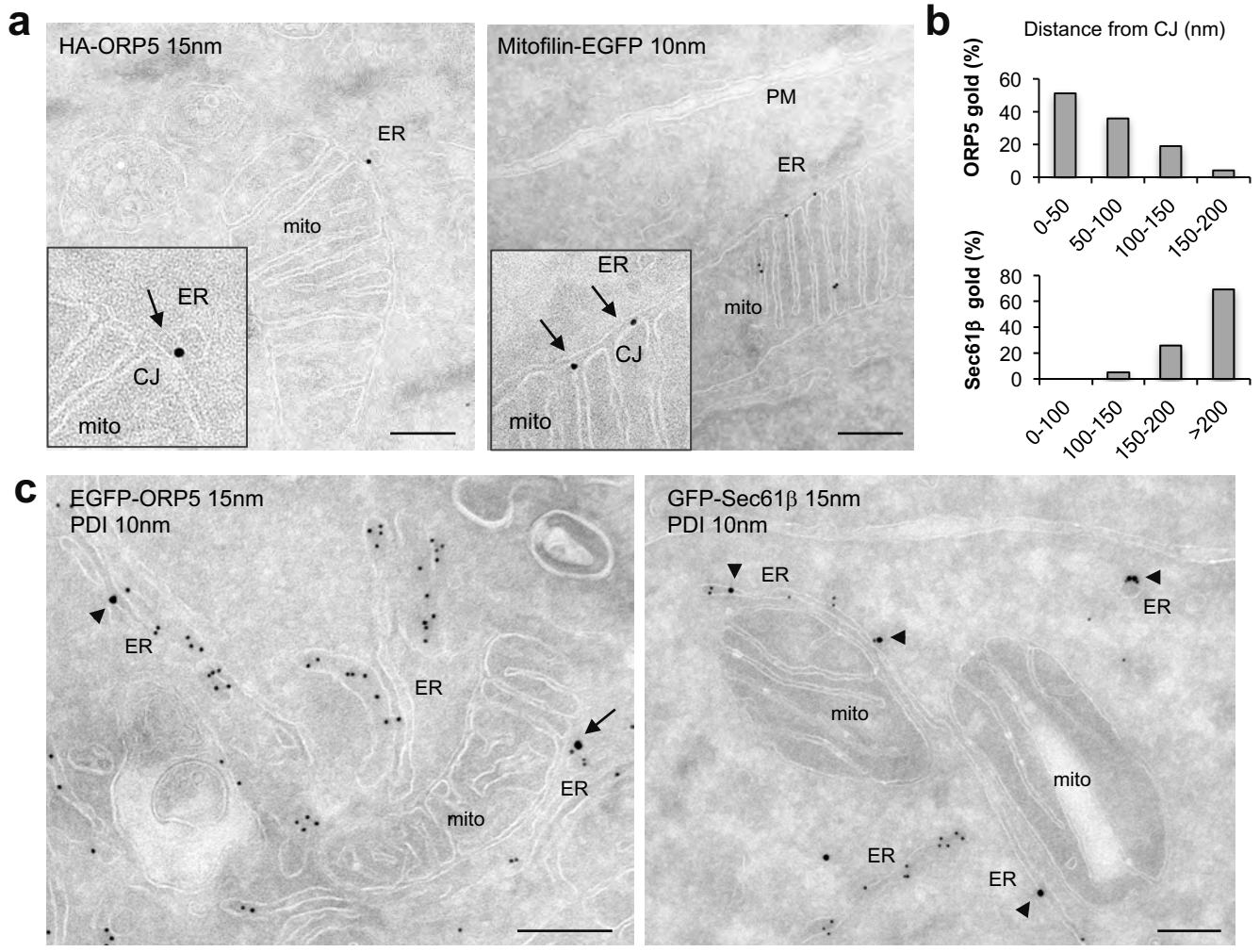

Figure 3. ORP5 localizes at ER-mitochondria contact sites near cristae junctions (CJ).

(a) Electron micrographs of ultrathin cryosections of HeLa cells transfected with HA-ORP5 or Mitofilin-EGFP and immunogold stained with anti-HA or anti-GFP (10 or 15 nm gold), showing ORP5 localization at ER-mitochondria contacts in close proximity to CJ (arrow) and the localization of the MICOS complex (Mitofilin) at CJ (arrows). Scale bar 250 nm. (b) Quantification of the proximity of HA-ORP5 and EGFP-Sec61β gold particles to the CJ. Results are presented as the percentage of ORP5 or Sec61b gold particles at specific ranges of distance (in nm) from CJ. 150 gold particles were counted on randomly selected cell profiles in each sample. (c) Electron micrographs of ultrathin cryosections of HeLa cells transfected with EGFP-ORP5 or GFP-Sec61β and immunogold labeled with anti-GFP (15 nm gold) and anti-PDI (10nm gold). Note ORP5 localization at ER-mitochondria contacts near CJ (arrow) and Sec61β localization to ER membranes not in contact with the mitochondria membranes (arrowheads). Scale bar 250 nm.

Figure 3

a

Mass-Spectrometry Analysis

		IP EGFP	IP EGFP-ORP5	IP EGFP-ORP5ΔPH
Protein	**Localization**	**Mascot Score**		
ORP5	MAMs	0	9689	12192
ORP8	MAMs	31	930	690
Mitofilin	IMM	43	579	1150
SAM50	OMM	0	237	516
Metaxin2	OMM	0	32	175
RHOT2	OMM	0	131	119
TOM22	OMM	0	77	95
PSS1	MAMs	0	150	200
PTPIP51	OMM	0	76	73

b

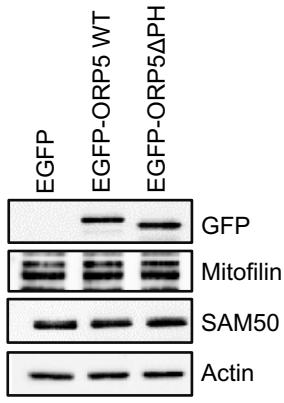

c

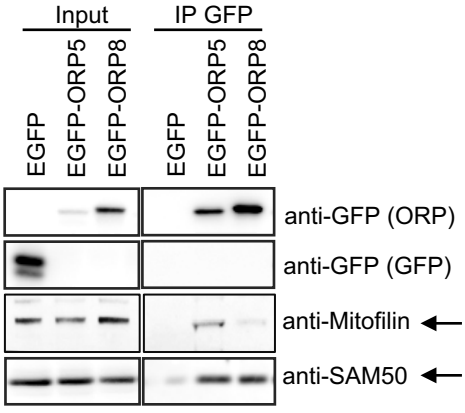

d

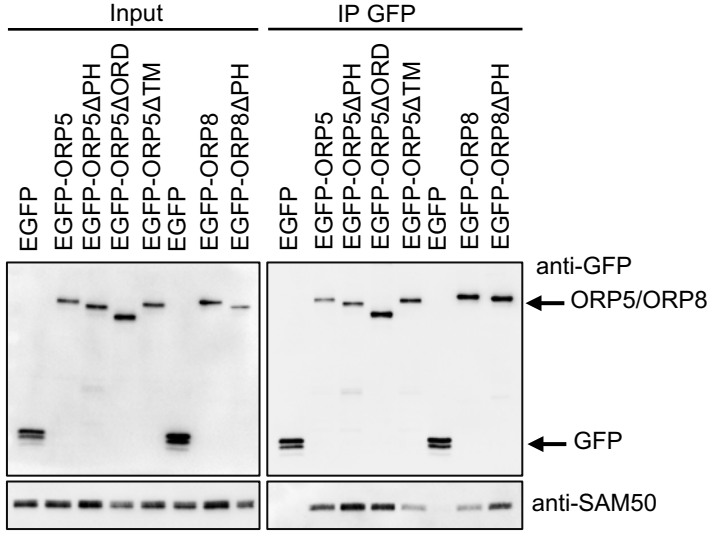

e

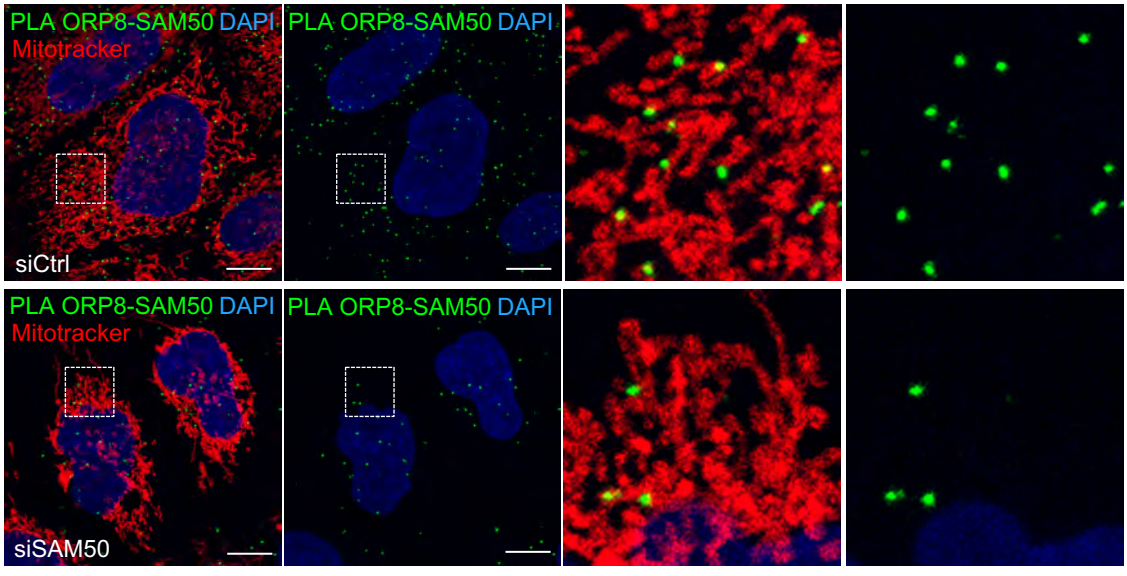

f

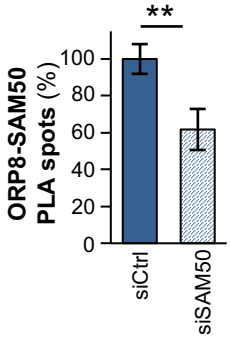

g

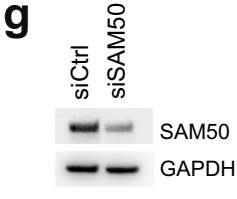

Figure 4

Figure 4. ORP5 and ORP8 interact with the MIB/MICOS complex at ER-mitochondria contacts. (a) Identification of mitochondrial proteins associated to mitochondrial outer or inner membranes (OMM, IMM) that interact with EGFP-tagged ORP5 constructs by mass spectrometry. Note the presence of some proteins of the MIB complex: Mitofilin, SAM50 and Metaxin2 and of their interacting partner RHOT2. Interaction scores (Mascot scores) of Mitofilin, SAM50 and Metaxin2 with the EGFP-ORP5ΔPH construct are stronger than with EGFP-ORP5. (b) WB analysis showing GFP (EGFP-tagged constructs), Mitofilin, SAM50 and Actin levels in protein lysates from HeLa cells transfected with either EGFP (Control) or with EGFP-ORP5 or EGFP-ORP5ΔPH constructs. (c) EGFP-ORP5, EGFP-ORP8 or EGFP alone were transfected in HeLa cells then immuno-precipitated from lysates and analyzed by western blot using antibodies against GFP (for ORP5 or ORP8), Mitofilin or SAM50. (d) EGFP-ORP5, EGFP-ORP5ΔPH, EGFP-ORP5ΔORD, EGFP-ORP5ΔTM, EGFP-ORP8, EGFP-ORP8ΔPH or EGFP alone were transfected in HeLa cells then immuno-precipitated from lysates and analyzed by western blot using antibodies against GFP (for ORP5 or ORP8) or against SAM50. (e) Confocal images of Ctrl (siCtrl) and SAM50 (siSAM50) knockdown HeLa cells showing endogenous interaction of ORP8-SAM50 by Duolink PLA (green) at MAMs. Mitochondria are labeled by MitoTracker (red) and nuclei by DAPI (blue). Images are presented as maximum projection of all layers. Insets show magnifications of the boxed regions. Scale bar, 10 μm. (f) Quantification of ORP8-SAM50 PLA signals in Control and SAM50 knockdown HeLa cells, showing the reduction of about 50% of ORP8-SAM50 PLA in SAM50 knockdown cells as compared to control. Bars indicate mean values ±SEM. Number of cell analysed: siCtrl (n=30), siSAM50 (22) Statistical analysis: P values were determined by unpaired student's t-test, **P<0.01. (g) WB analysis showing SAM50 and GAPDH levels in protein lysates from siCtrl and siSAM50 cells.

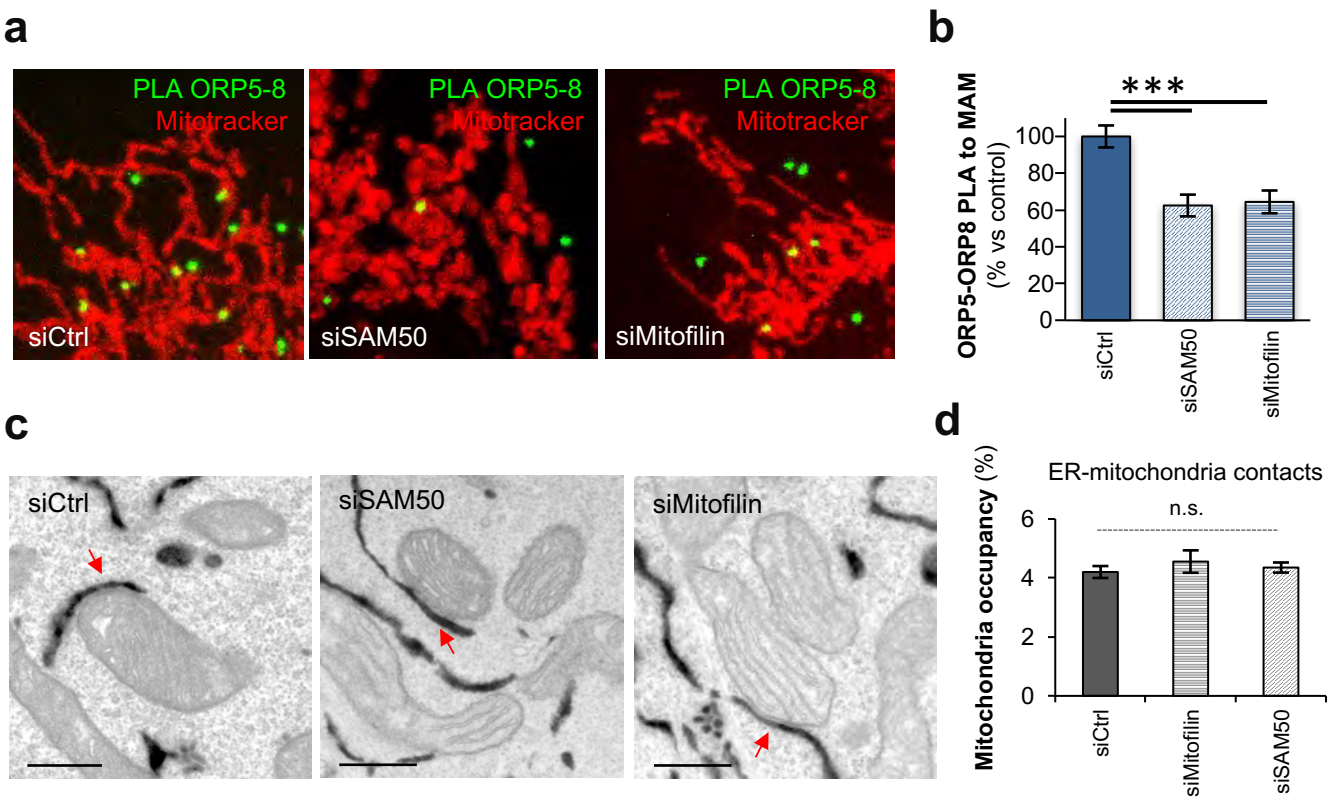

Figure 5. SAM50 and Mitofilin knockdowns induce a decrease in ORP5-8 interaction at MAMs but do not alter the abundance of ER-mitochondria contact sites. (a) Confocal images of a region of Ctrl (siCtrl), SAM50 (siSAM50) and Mitofilin (siMitofilin) knockdown HeLa cells showing endogenous interaction of ORP5-8 by Duolink PLA (green) near mitochondria (MitoTracker, red). (b) Quantification of ORP5-8 PLA signals in Control, SAM50 and Mitofilin knockdown HeLa cells, showing the decrease of about 40% of ORP5-ORP8 PLA in SAM50 and Mitofilin knockdown cells as compared to control. Bars indicate mean values ±SEM. Number of cell analysed: siCtrl (n=33), siSAM50 (n=19), siMitofilin (n=24). Statistical analysis: unpaired sudent's *t*-test. ***P<0.001.(c) Representative electron micrographs of HeLa cells treated with Ctrl siRNAs or siRNAs against SAM50 or Mitofilin and transfected with HRP-KDEL. Red arrows indicate ER-mitochondria contact sites. Scale bar, 500 nm. (d) Quantifications of the extent of ER-mitochondria contact sites in Ctrl, Mitofilin and SAM50 knockdown cells expressing HRP-KDEL. Data are shown as % of the ER in contact with mitochondria (mitochondria occupancy) ±SEM, n = 30 for siCtrl, n = 20 cell profiles for siMitofilin and siSAM50 and 1000 mitochondria; n.s; not significant.

Figure 5

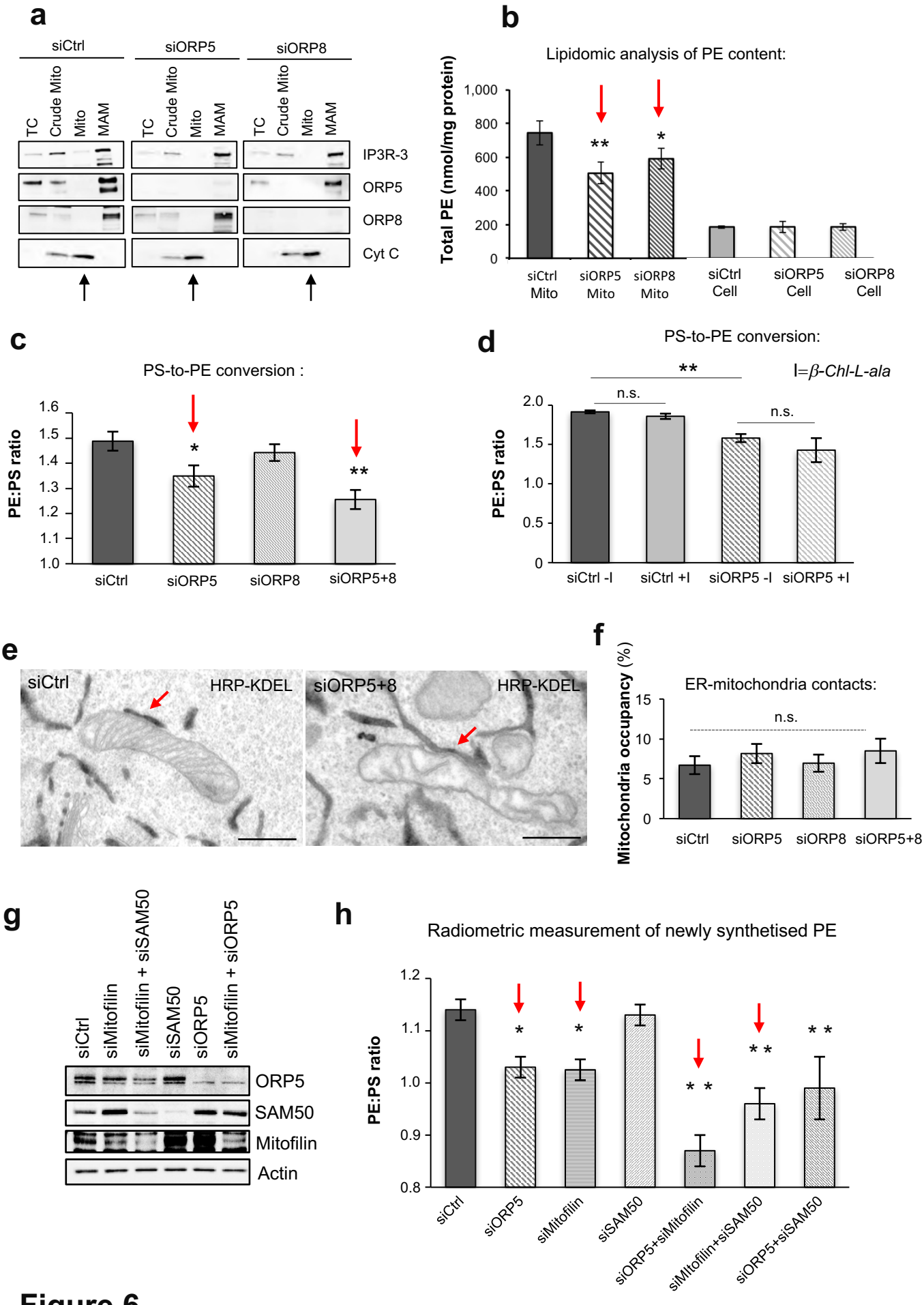
a
siCtrl
siORP5
siORP8
TC
Crude Mito
Mito
MAM
IP3R-3
ORP5
ORP8
Cyt C
b
Lipidomic analysis of PE content:
Total PE (nmol/mg protein)
1,000
800
600
400
200
0
siCtrl Mito
siORP5 Mito
siORP8 Mito
siCtrl Cell
siORP5 Cell
siORP8 Cell
c
PS-to-PE conversion :
PE:PS ratio
1.6
1.5
1.4
1.3
1.2
1.1
1.0
siCtrl
siORP5
siORP8
siORP5+8
d
PS-to-PE conversion:
I=β-Chl-L-ala
n.s.
PE:PS ratio
2.0
1.5
1.0
0.5
0
siCtrl -I
siCtrl +I
siORP5 -I
siORP5 +I
e
siCtrl
HRP-KDEL
siORP5+8
HRP-KDEL
f
ER-mitochondria contacts:
Mitochondria occupancy (%)
15
10
5
0
n.s.
siCtrl
siORP5
siORP8
siORP5+8
g
siCtrl
siMitofilin
siMitofilin + siSAM50
siSAM50
siORP5
siMitofilin + siORP5
ORP5
SAM50
Mitofilin
Actin
h
Radiometric measurement of newly synthetised PE
PE:PS ratio
1.2
1.1
1.0
0.9
0.8
siCtrl
siORP5
siMitofilin
siSAM50
siORP5+siMitofilin
siMitofilin+siSAM50
siORP5+siSAM50

Figure 6

Figure 6. ORP5/8 and the MIB/MICOS complex regulate levels of PS-derived mitochondrial PE (a) Crude mitochondria, mitochondria, and MAM fractions were purified from Ctrl, ORP5 and ORP8 siRNA-treated HeLa cells. Equal amounts of protein from each fraction were loaded on a 4–20% gradient SDS–PAGE gel and immunoblotted using anti-ORP5, anti-ORP8, anti-IP3R-3 (MAM protein), and anti-cytochrome c (mitochondrial protein). Mito, mitochondria; MAM, mitochondria-associated ER membrane. (b) Mass spectrometry (MS)-based quantification of the PE content (nmol/mg protein) of mitochondria isolated from Ctrl, ORP5 or ORP8 knockdown cells and of Ctrl, ORP5 or ORP8 knockdown intact cells. Data are shown as mean of three independent replicates ±SEM. Statistical analysis: unpaired student's *t*-test, *P<0.05, **P<0.01. (c) HeLa cells transfected with siCtrl, siORP5, siORP8 or siORP5+ORP8 RNAi oligos were incubated with L-[^{3}H(G)]serine (30.9 Ci/mmol) for 18 hours. After extraction and separation of lipids by TLC, PS and PE spots were scraped and analyzed for [^{3}H] radioactivity, as described under "Methods". Each condition was analyzed in triplicate in each of three independent biological replicates. Data are presented as mean of PE:PS ratio ±SEM. Statistical analysis: unpaired student's *t*-test, *P<0.05, **P<0.01 compared to Ctrl. (d) Cells transfected with siCtrl and siORP5 oligos were treated with b-Chloro-L-alanine (b-Chl-L-ala, inhibitor of Ser-palmitoyltransferase) or untreated, then pulsed with 15 µCi/ml of [^{3}H(G)]serine for 1 hour and chased for 12 hours in serum-free DMEM, before analysis. n.s. not significant, **P<0.01 compared to Ctrl. (e) Electron micrographs of HRP-KDEL-expressing HeLa cells treated with Ctrl siRNAs (siCtrl) or siRNAs against ORP5 and ORP8 (siORP5+siORP8). Red arrows indicate ER-mitochondria contact sites. Scale bar, 500 nm. (f) Quantifications of the extent of ER-mitochondria contact sites in siCtrl, siORP5, siORP8 and siORP5+8 cells expressing HRP-KDEL. Data are shown as % of the ER in contact with mitochondria (mitochondria occupancy) ±SEM, n = 20 cell profiles and ±900 mitochondria; n.s; not significant. (g) Western analysis showing ORP5, SAM50, Mitofilin and Actin levels in protein lysates from HeLa cells treated with siRNA against Ctrl, ORP5, Mitofilin or SAM50. Arrow indicates the specific band for Mitofilin.

(h) Radiometric measurement of PS-to-PE conversion in the indicated siRNAs. Data are presented as mean of PE:PS ratio ±SEM. Each condition was performed in triplicate in each of the independent biological replicates (n = 5 for siCtrl and siORP5; n = 4 for siSAM50; n = 3 for the other siRNAs conditions). Statistical analysis: unpaired student's *t*-test , *P<0.05, **P<0.01 compared to Ctrl.

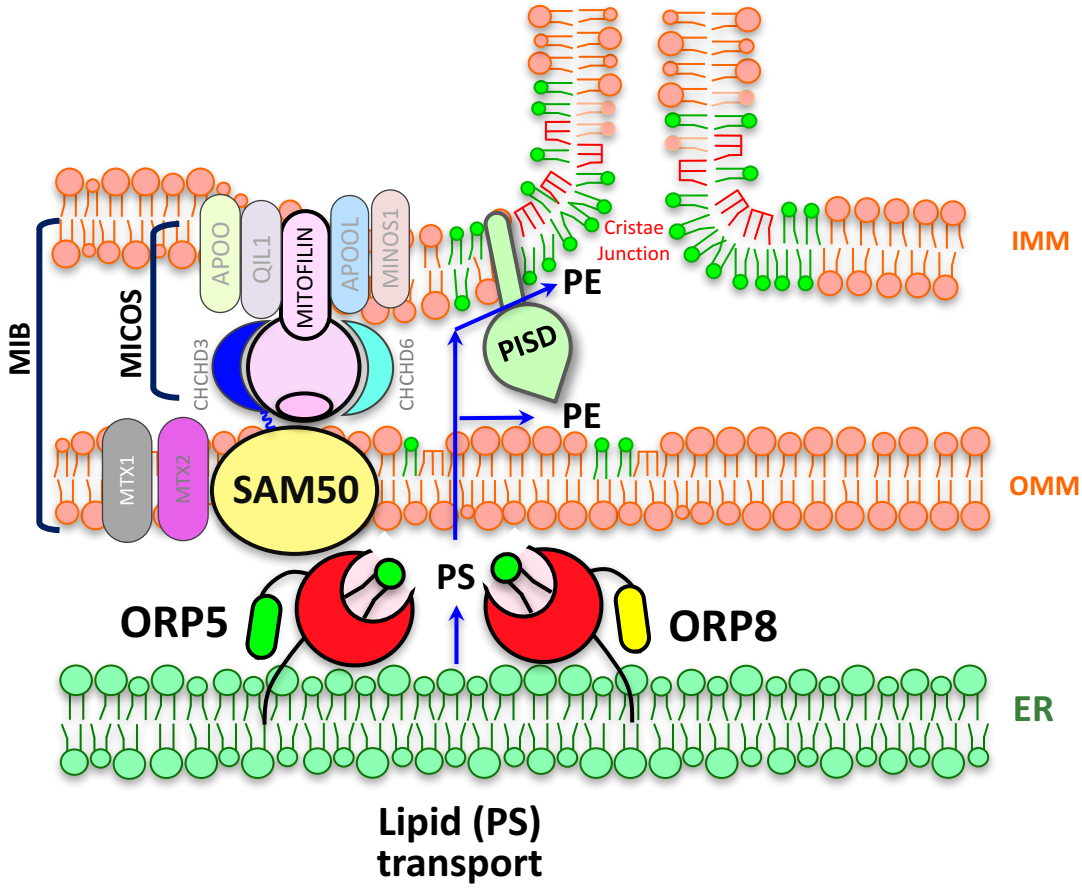

Figure 7. PS transport at ER-mitochondria contact site subdomains associated to MIB/MICOS complex. ORP5/8 mediate the transfer of PS from ER to mitochondria at ER-mitochondria membrane contact sites. This transfer occurs at ER subdomains facing the cristae junctions (CJ) where ORP5/8 interacts with SAM50 and Mitofilin, key proteins of the MIB complex. This interaction facilitates the transfer of PS from ER to the mitochondrial membranes at the level of CJ and PS conversion into PE, a phospholipid that plays a critical role in cristae organization and mitochondrial function.

Figure 7

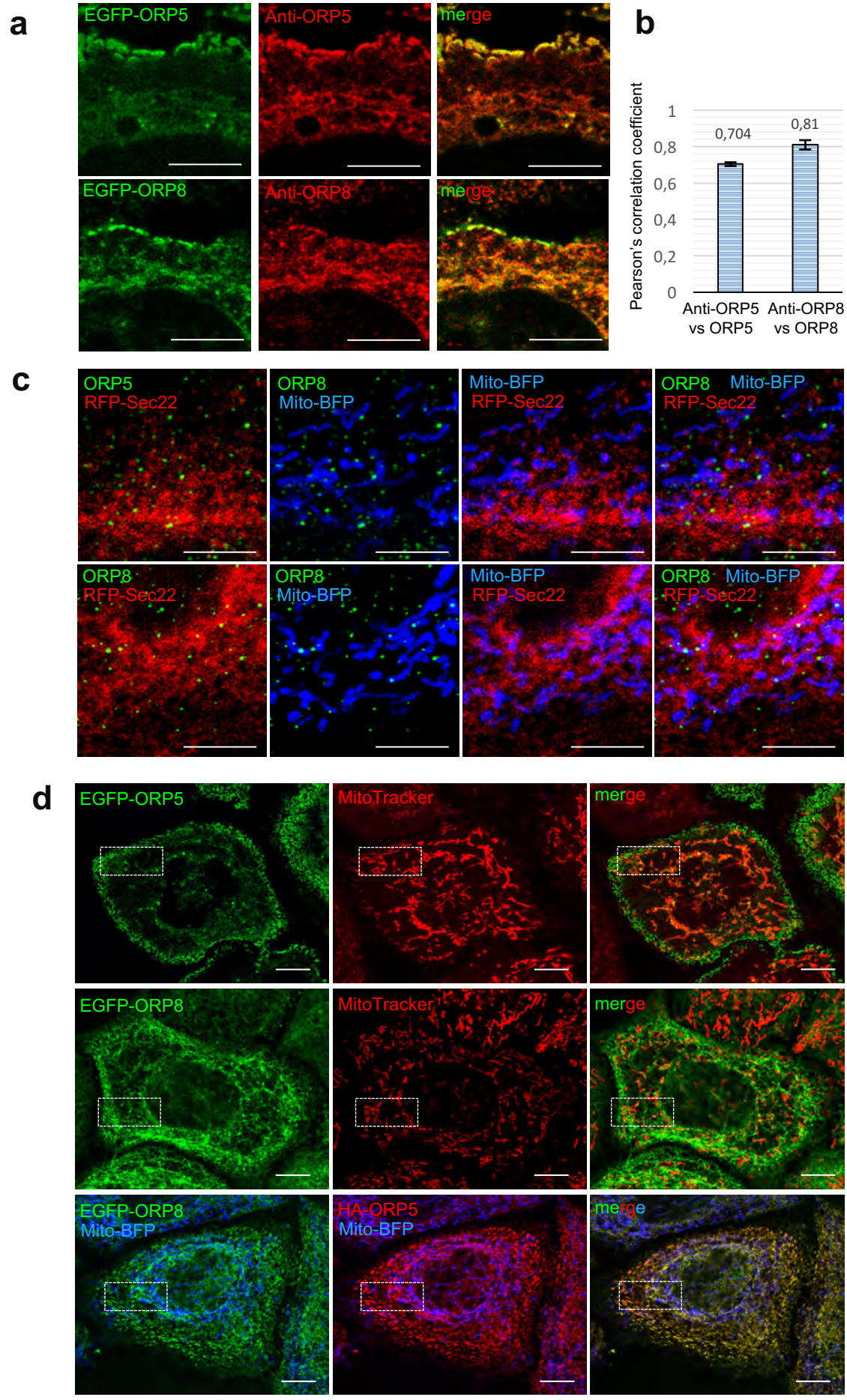
a
EGFP-ORP5
Anti-ORP5
merge
EGFP-ORP8
Anti-ORP8
merge
b
Pearson's correlation coefficient
1
0,8
0,6
0,4
0,2
0
0,704
0,81
Anti-ORP5 vs ORP5
Anti-ORP8 vs ORP8
c
ORP5
RFP-Sec22
ORP8
Mito-BFP
Mito-BFP
RFP-Sec22
ORP8
Mito-BFP
RFP-Sec22
ORP8
RFP-Sec22
ORP8
Mito-BFP
Mito-BFP
RFP-Sec22
ORP8
Mito-BFP
RFP-Sec22
d
EGFP-ORP5
MitoTracker
merge
EGFP-ORP8
MitoTracker
merge
EGFP-ORP8
Mito-BFP
HA-ORP5
Mito-BFP
merge

Figure S1

Figure S1. Endogenous and co-overexpressed ORP5 and ORP8 co-localize at ER-mitochondria contact sites. (a) Confocal images of a region of HeLa cell transfected with EGFP-ORP5 (green) or EGFP-ORP8 (green) and immunostained using anti-ORP5 (red) or anti-ORP8 (red) antibodies. Scale bar, 5 μm. (b) Quantifications of the colocalization (Pearson's factor) of EGFP-ORP5 or EGFP-ORP8 with anti-ORP5 or anti-ORP8. Bars indicate mean values ±SEM. Cells analyzed for sample: n=5. (c) Confocal micrographs of regions of HeLa cell transfected with RFP-Sec22b (red) together with Mito-BFP (blue) and immunostained for anti-ORP5 (green) or anti-ORP8 (green) antibodies. Scale bar, 5 μm. (d**)** Confocal micrograph of a HeLa cell transfected with EGFP-ORP5 (green), EGFP-ORP8 (green) or EGFP-ORP8 (green) + HA-ORP5 (anti-HA, red), together with Mito-BFP (blue). The boxed areas are magnified in Fig 1g. Scale bar, 10 μm.

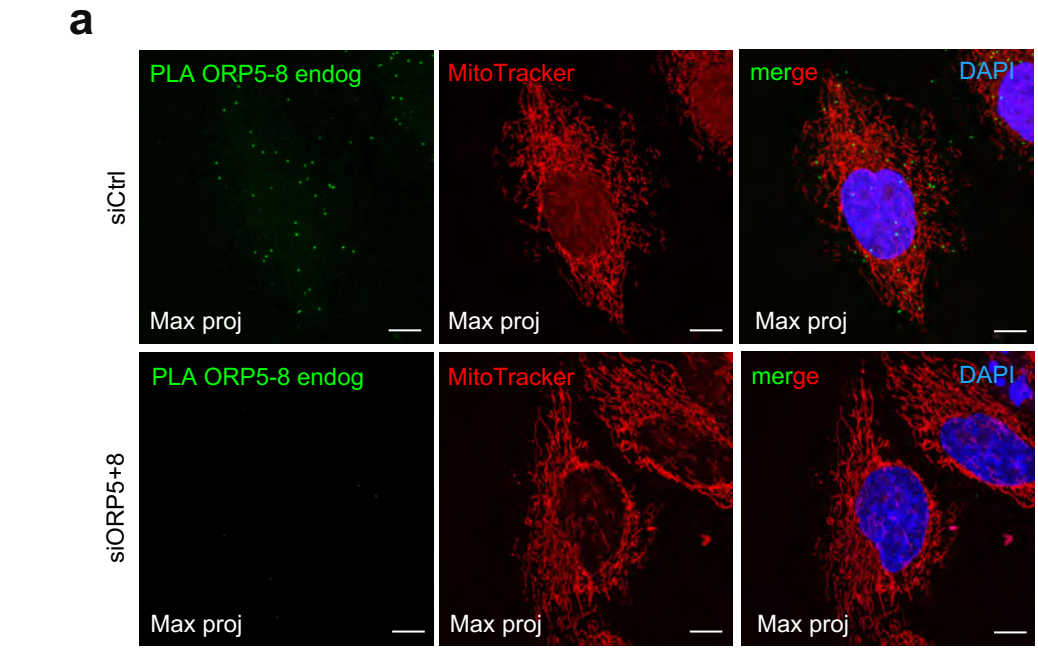
a
PLA ORP5-8 endog
MitoTracker
merge
DAPI
siCtrl
siORP5+8
Max proj

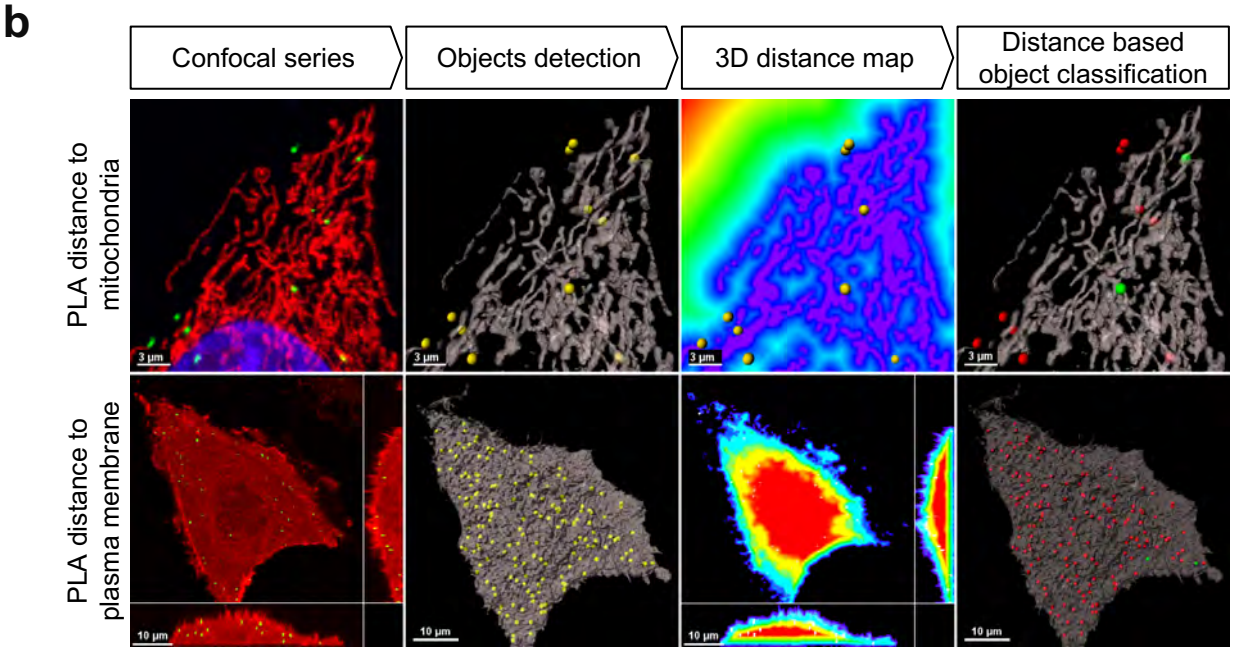
b
Confocal series
Objects detection
3D distance map
Distance based object classification
PLA distance to mitochondria
PLA distance to plasma membrane
3 µm
10 µm

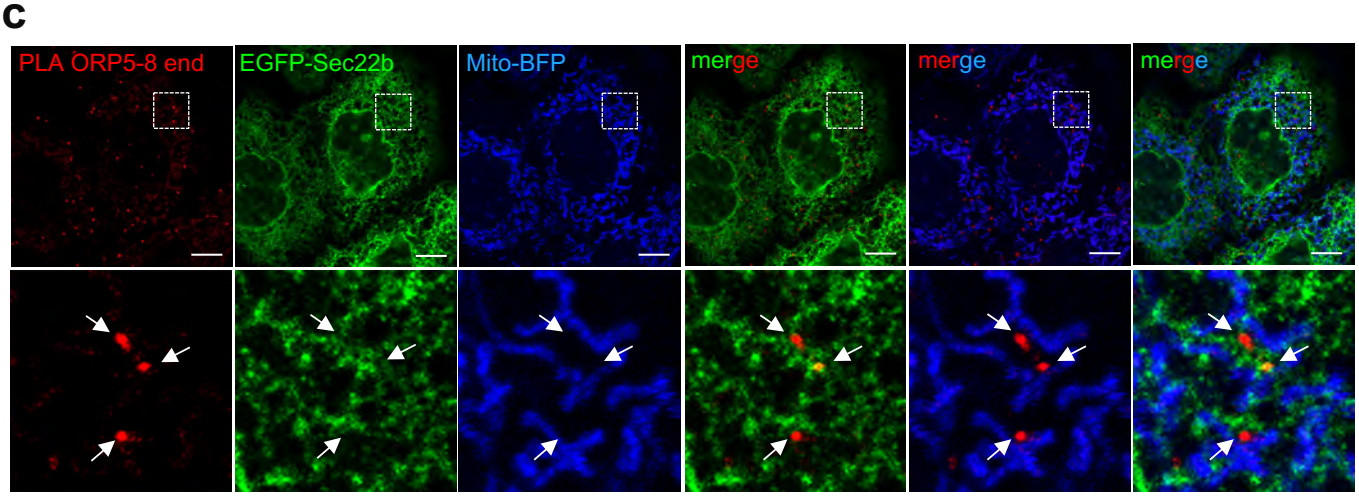
c
PLA ORP5-8 end
EGFP-Sec22b
Mito-BFP
merge
merge
merge

Figure S2

Figure S2. Endogenous ORP5-ORP8 interaction at ER-mitochondria contact sites. (a**)** Confocal images showing endogenous interaction of ORP5-8 by Duolink PLA (green) in Ctrl (siCtrl), and ORP5+ORP8 (siORP5+8) knockdown HeLa cells labeled with MitoTracker (red) to stain mitochondria. Images are presented as maximum projection of all layers. Insets show magnifications of the boxed regions. Scale bar, 10 µm. (b) Workflow for the identification of PLA signals in close proximity to the mitochondria or plasma membrane. First the confocal stacks are segmented to identify the PLA foci (spots), the mitochondria network (surfaces), and the plasma membrane (cells). Then 3D distance maps are computed towards the outside of the surfaces (mitochondria) or inside the cells allowing the measurement of the distance of each spot from the closest mitochondria or membrane. Finally PLA spots are classified into two population (red and green) based on a proximity threshold of 380nm established on the precision of the detection system. (c) Confocal micrographs of HeLa cell transfected with GFP-Sec22b (green) and Mito-BFP (blue) and showing endogenous interaction of ORP5-8 by Duolink PLA (red). Images are presented as superposition of two layers. Scale bar, 5 µm.

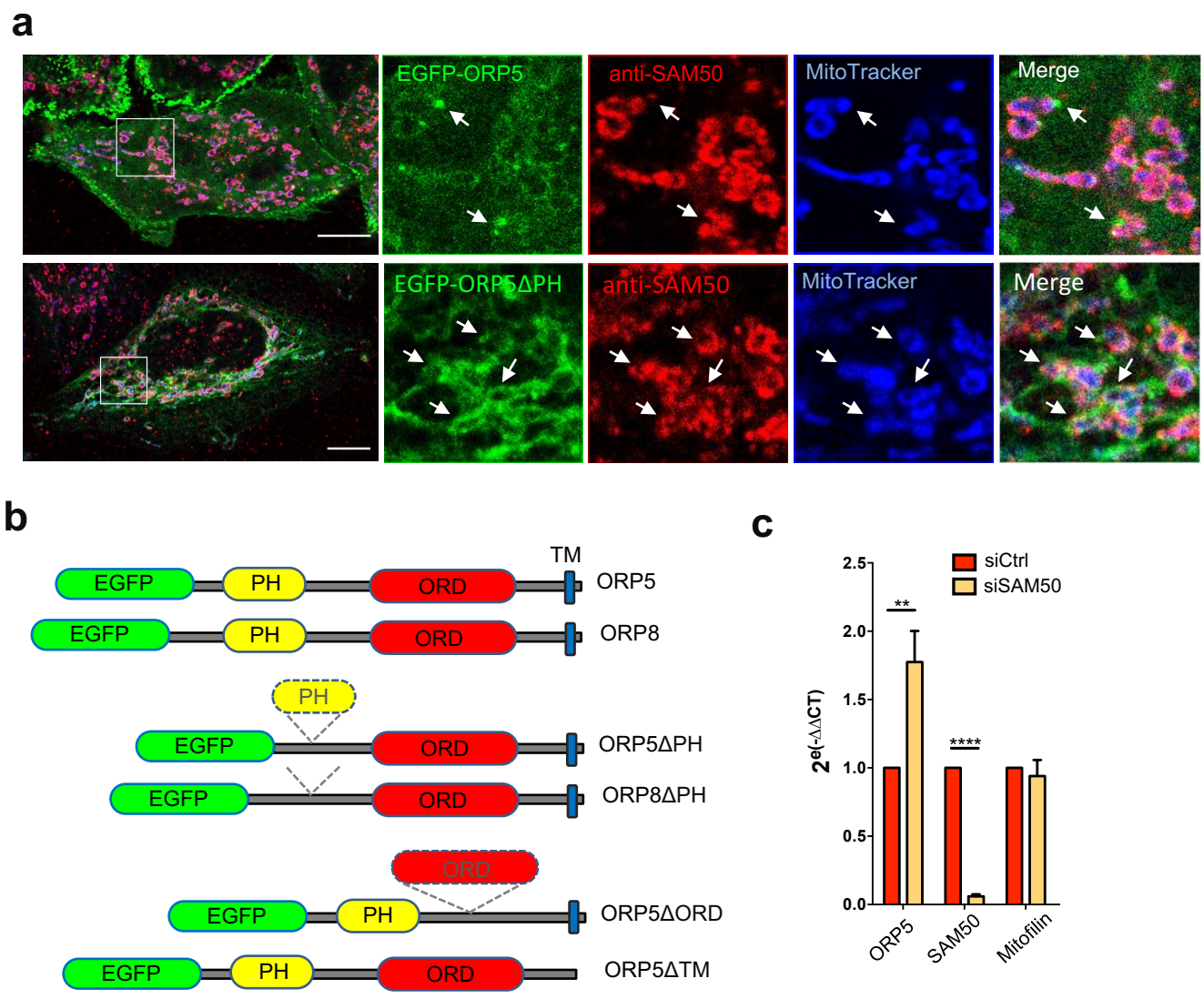

Figure S3. Localization of ORP5 near SAM50-labeled mitochondria and effect of SAM50 KD on ORP5 and Mitofilin transcription. (a) Confocal micrograph of a HeLa cells transfected with EGFP-ORP5 or EGFP-ORP5ΔPH (green) and Mito-BFP (blue) and stained with anti-SAM50 (red) antibody. Insets show magnifications of the boxed regions. Scale bar, 10 μm. (b) ORP5 and ORP8 full-length and mutant constructs used in Fig 4a-d and in in Fig. EV3a. (c) Quantitative RT-PCR analysis of ORP5, SAM50 and Mitofilin in SAM50 knockdown cells versus control HeLa cells. y axis: $2^{(-\Delta\Delta Ct)}$ value represents differences between the mean Ct (Cycle threshold) values of tested genes and those of reference gene (SDHA). SAM50 knockdown does not alter Mitofilin RNA levels and it induces an increase in ORP5 transcription. Statistical analysis: unpaired student's *t*-test , **P<0.01, ****P<0.0001.

Figure S3

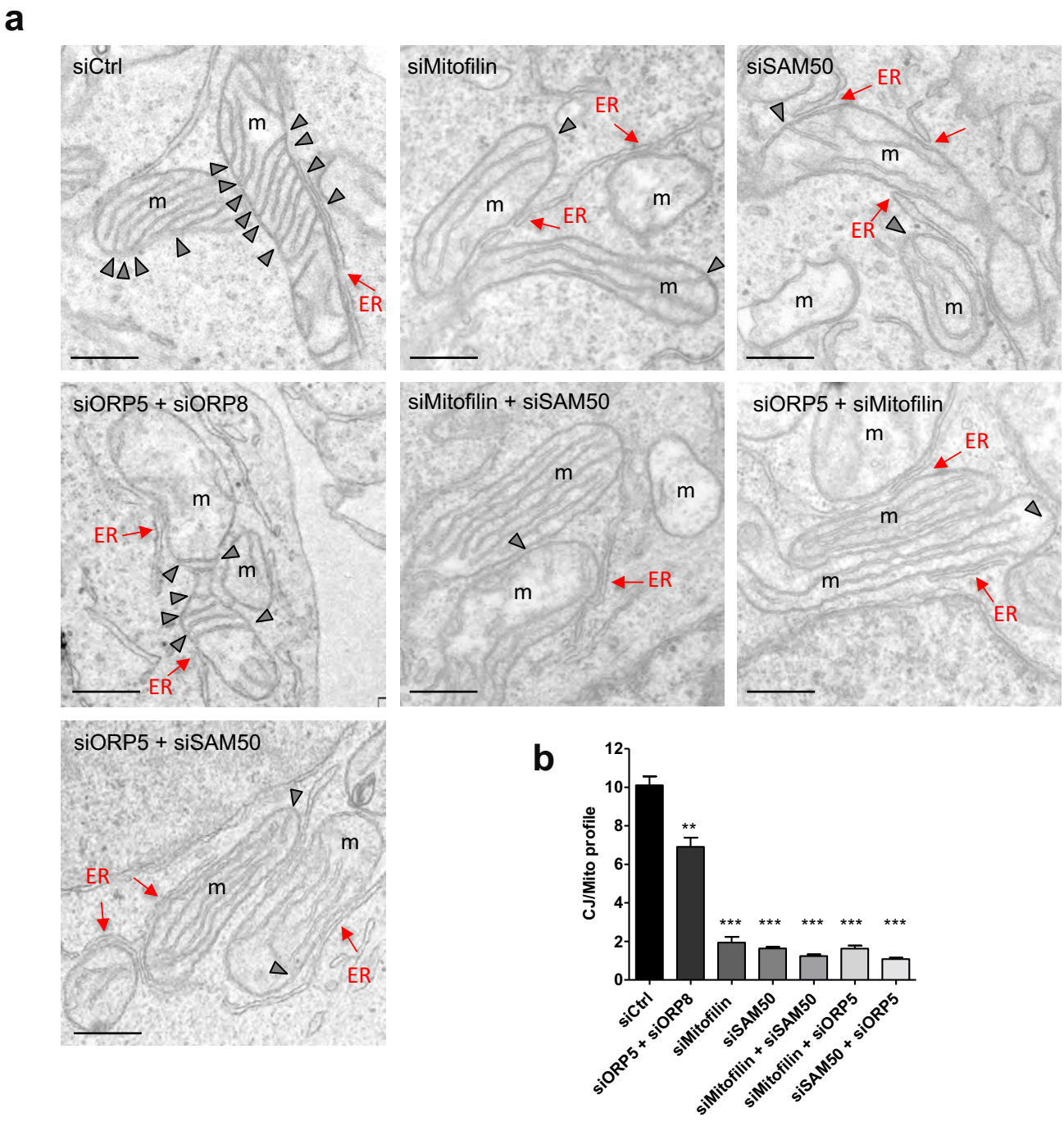

Figure S4. Cristae Junctions are altered upon SAM50, Mitofilin and ORP5+8 knockdowns. (a) Representative EM micrographs showing the morphology of mitochondria in HeLa cells treated with siRNA against ORP5, ORP8, Mitofilin and SAM50. Scale bar, 200 nm. Red arrows indicate ER elements in contact with mitochondria; arrowheads indicate CJ; m, mitochondria. (b) Quantifications of the number of CJ per mitochondria profile in the indicated siRNA conditions. % of CJ ±SEM, n = 170-260 mitochondria. Statistical analysis: unpaired student's *t*-test , **P<0.01, ***P<0.001.

Figure S4

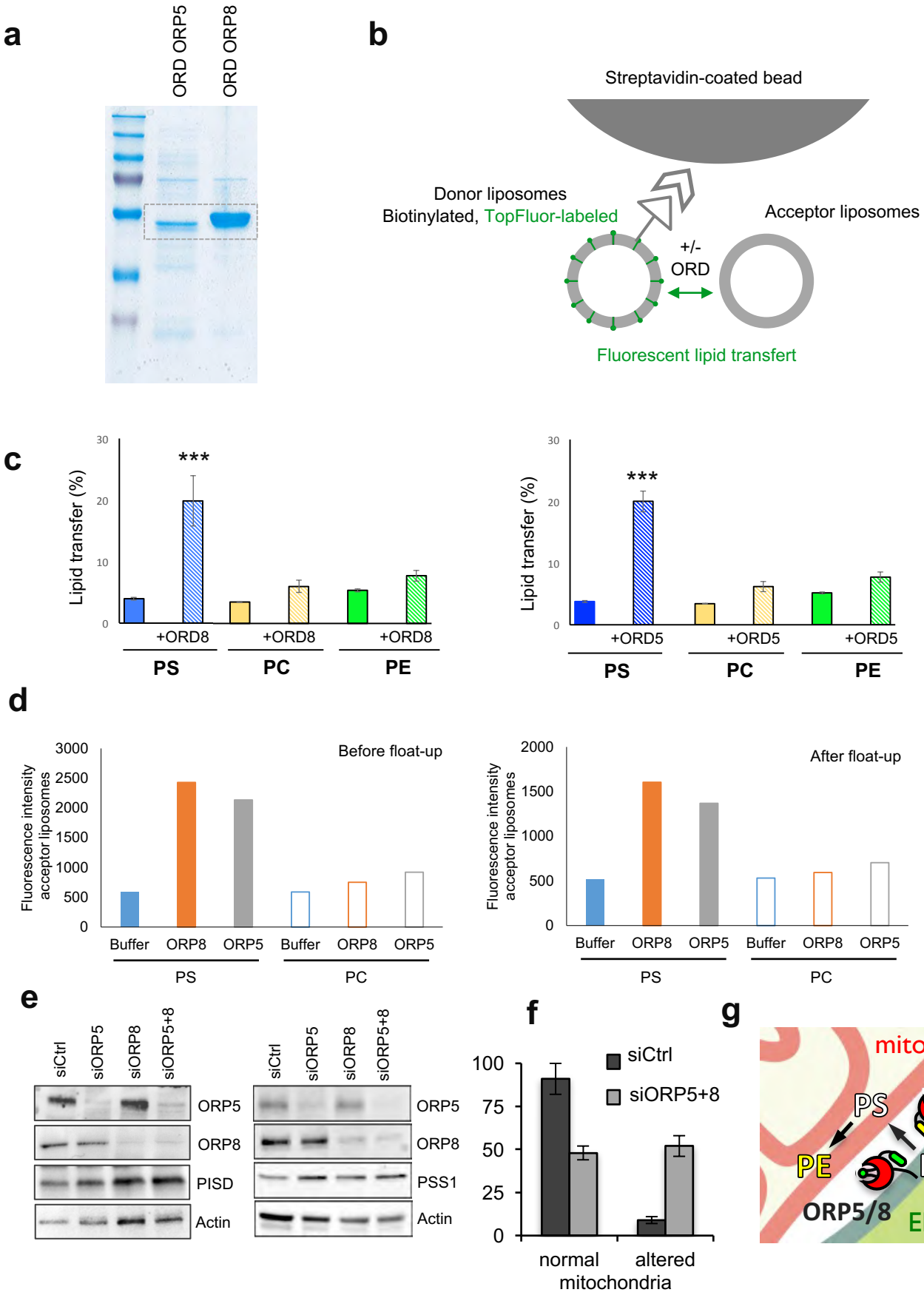
a
ORD ORP5
ORD ORP8
b
Streptavidin-coated bead
Donor liposomes
Biotinylated, TopFluor-labeled
Acceptor liposomes
+/-
ORD
Fluorescent lipid transfert
c
Lipid transfer (%)
***
+ORD8
PS
PC
PE
+ORD5
d
Before float-up
After float-up
Fluorescence intensity acceptor liposomes
Buffer
ORP8
ORP5
e
siCtrl
siORP5
siORP8
siORP5+8
ORP5
ORP8
PISD
PSS1
Actin
f
siCtrl
siORP5+8
normal mitochondria
altered mitochondria
g
mito
PS
PE
ORP5/8
ER

Figure S5

Figure S5. ORP5 and ORP8 ORD domains mediate PS transfer between liposomes *in vitro* and ORP5/8 knockdown alter mitochondria morphology but not PSD1, PSS1 protein levels *in situ*. (a) Coomassie stained SDS-PAGE of the recombinant ORD domain of ORP5/8 proteins purified from BL21DE3 RILP cells. (b) Schematic cartoon of the *in vitro* assay used to study ORP5/8 ORD-mediated lipid transport between liposomes. (c) Donor liposomes containing fluorescent lipids (97 mol% POPC, 1 mol% TopFluor-PS, -PC or -PE and 2 mol% of biotinylated-PE) and pre-bound to streptavidin beads were mixed at a 1:1 molar ratio with acceptor liposomes (100 mol% POPC) in the presence or absence of ORP5 or ORP8 ORD domains (250 µM of donor and acceptor liposomes and 0,3 µM of proteins in the reaction solution). The increase in fluorescence in the acceptor liposomes, which remain unbound in the solution, was measured after 1 hour of incubation at 37° C. Data are presented as % of transferred lipid ±SEM and are the mean of six independent experiments. Statistical analysis: unpaired student's *t*-test , ***P<0.001. (d) Results of a lipid transfer experiment performed as in Fig. EV5c and presented as the fluorescence intensity of acceptor liposomes before (left panel) or after (right panel) their floatation on a Nycodenz gradient to confirm that fluorescence comes from the liposomes membrane. (e) WB analysis showing ORP5, ORP8, PSD1, PSS1 and Actin levels in protein lysates from HeLa cells treated with either Ctrl siRNAs or with siRNAs against ORP5 or/and ORP8. (f) Quantifications of the number of mitochondria with aberrant cristae morphology in the indicated siRNA conditions. Data are shown as % of mitochondria ±SEM, n = 20 cell profiles and ±700 mitochondria. Statistical analysis: unpaired student's *t*-test, **P<0.01 compared to siCtrl. (g) Schematic representation of non-vesicular PS transfer mediated by ORP5/8 at ER-mitochondria contact sites. PS is transported to mitochondrial membranes where it is rapidly converted into mitochondrial PE.

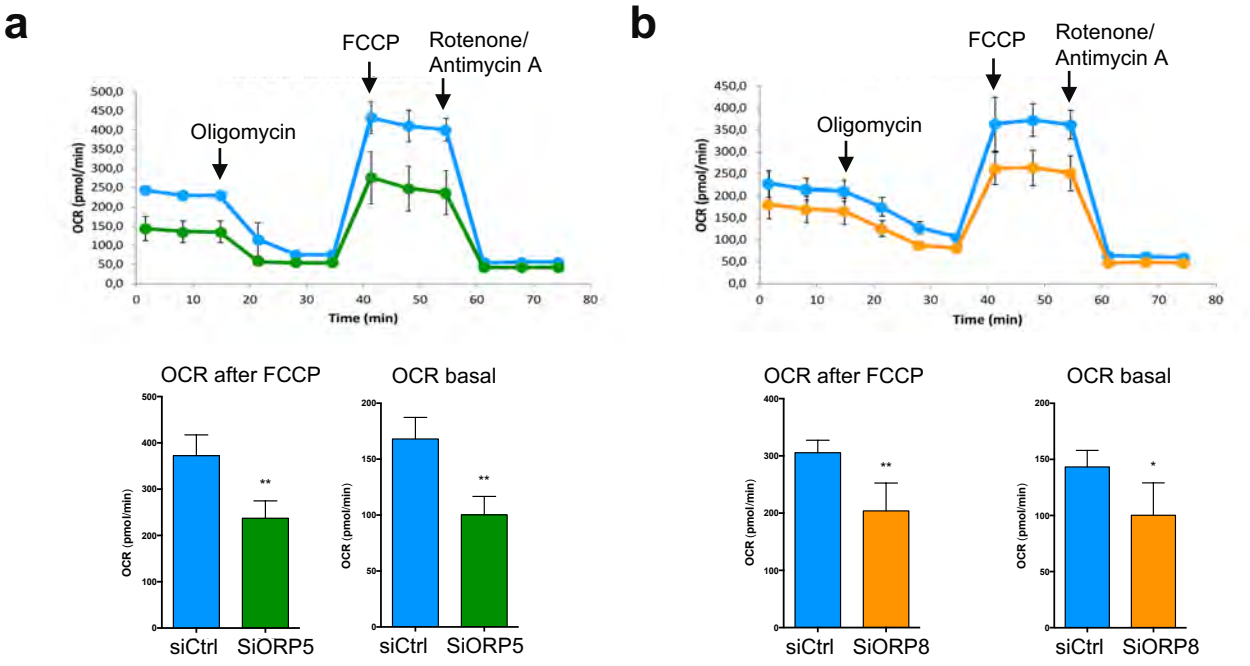

Figure S6. ORP5 and ORP8 knockdowns affect mitochondria respiratory function. (a-b) Mitochondrial oxygen consumption rate (OCR) measured in Ctrl and ORP5 (a) or ORP8 (b), siRNA-treated HeLa cells. OCR trace was obtained by sequential measurement of basal OCR (OCR_{BAS}), OCR after the addition of Oligomycin, OCR after the addition of FCCP (OCR_{FCCP}) and OCR after the addition of Rotenone/Antimycin A. Note the reduced OCR in siORP5 and siORP8 cells compared to Ctrl siRNA cells. Error bars denote ±SEM. Data shown in the bar charts are the mean of 4 independent repeats (n=4). Statistical analysis: unpaired student's *t*-test, *P<0.05, **P<0.01 compared to Ctrl.

Figure S6